UNLV University Libraries
University of Nevada, Las Vegas

12-1-2012

2000 Year Moisture Source Record from a Central Nevada Speleothem

Paul Pribyl

University of Nevada, Las Vegas, paul.pribyl@gmail.com

Follow this and additional works at: https://digitalscholarship.unlv.edu/thesesdissertations

Part of the Atmospheric Sciences Commons, Climate Commons, and the Geology Commons

2000 YEAR MOISTURE SOURCE RECORD FROM

A CENTRAL NEVADA SPELEOTHEM

By

Paul Edward Pribyl

Bachelor of Science
University of Wyoming
2010

A thesis submitted in partial fulfillment
of the requirements for the

Master of Science in Geoscience

Department of Geoscience
College of Sciences
The Graduate College

University of Nevada, Las Vegas
December 2012

THE GRADUATE COLLEGE

We recommend the thesis prepared under our supervision by

Paul Pribyl

entitled

2000 Year Moisture Source Record from a Central Nevada Speleothem

be accepted in partial fulfillment of the requirements for the degree of

Master of Science in Geoscience
Department of Geoscience

Matthew Lachniet, Ph.D., Committee Chair

David Kreamer, Ph.D., Committee Member

Zhongbo Yu, Ph.D., Committee Member

Stanley D. Smith, Ph.D., Graduate College Representative

Tom Piechota, Ph.D., Interim Vice President for Research &
Dean of the Graduate College

December 2012

ABSTRACT

2000 year moisture source record from a central Nevada speleothem

by

Paul Pribyl

Dr. Matthew Lachniet, Examination Committee Chair
Professor of Geoscience
University of Nevada, Las Vegas

The goal of this study was to determine the moisture source of winter precipitation in the central Great Basin for the past 2000 years, and to elucidate the role of Pacific Ocean and North American climate variability modes in driving observed droughts of the region around the Medieval Climatic Anomaly (MCA, ~900-1300 CE). Here a high resolution (~2-4 year) precisely dated moisture source reconstruction is presented from the $\delta^{18}O$ values of speleothem LC-1 collected from Leviathan Cave in central Nevada, which reveals significant $\delta^{18}O$ variability. I attribute the $\delta^{18}O$ variability to changes in winter-season moisture circulation over the past 2000 years, which were likely forced by the Pacific/North American (PNA) teleconnection and associated ocean-atmosphere phenomena. I suggest that lower (higher) $\delta^{18}O$ values are indicative of increased (decreased) contribution northern-Pacific sourced moisture during winter months, and this was due to the presence of a more negative (positive) state of the PNA. It was found that during the MCA there was an increase in northern sourced precipitation resulting from the presence of a negative PNA state associated with droughts in the region.

ACKNOWLEDGEMENTS

TABLE OF CONTENTS

LIST OF TABLES

LIST OF FIGURES

CHAPTER 1

INTRODUCTION

Purpose of Study

Paleoclimate studies have shown much of western North America, including parts of the

Great Basin, experienced large precipitation variations during the past 2000 years, including

severe droughts that exceed those in the instrumental record in duration and intensity.

Evidence from lake-level reconstructions, as well as tree-ring studies, from the Sierra Nevada

indicate droughts were unusually severe and persistent during the Medieval Climatic Anomaly

(MCA), which spanned the time interval of ~900-1350 CE (Stine, 1990; Stine, 1994; Benson et al.,

2002; Cook et al., 2004; Cook et al., 2007; Kleppe et al., 2011). It has been suggested that

observed precipitation deficits resulted from changes in Pacific Basin circulations and related

atmospheric teleconnections (Hughes and Diaz, 1994; Stine, 1994; Cole et al., 2002; Jones and

Mann, 2004; Herweijer et al., 2006; Cook et al., 2007; Graham et al., 2007; Conroy et al., 2009) .

Teleconnections are associations and statistically verifiable correlations among climate

characteristics separated by distance.

The task of understanding present and past relationships within the global climate

system is becoming increasingly important as observations continue to support the idea of

anthropogenic influenced climate change. Projections for future climate conditions indicate a

transition to a more arid southwest with a 10% chance that live storage in Lake Mead and Lake

Powell will be gone by 2013 and a 50 % chance by 2021 (Seager et al., 2007; Barnett and Pierce,

2008). Such projections illustrate the need for a greater understanding between regional

drought occurrence and the energy (heat and moisture) transfer occurring within the atmosphere and ocean. Speleothems have been shown to be an appropriate proxy for reconstructing climate teleconnections (Lachniet, 2009). The oxygen isotopic composition of cave speleothems is largely dependent on the oxygen isotope ratio of cave drip water which is controlled by the isotopic ratio present in precipitation contributing to drip water recharge (Hendy, 1971; Lachniet, 2009).

Here a high resolution (~2-4 year) precisely dated moisture source reconstruction is presented. This reconstruction was created from the $\delta^{18}O$ values of a speleothem (LC-1) collected from Leviathan Cave in central Nevada. The goal of this study was to determine the moisture source of winter precipitation in the central Great Basin for the past 2000 years, and to elucidate the role of Pacific Basin circulations and North American climate variability modes in driving observed megadroughts of the region during the MCA. The dominant modes of climate variability that influence western North America are the Pacific/North American (PNA) teleconnection, El Niño/ Southern Oscillation (ENSO), and the Pacific Decadal Oscillation (PDO). The state of these climate modes has a strong influence on moisture origin across North America and it has been shown there is a strong correlation between moisture source and the isotopic composition of precipitation in the region (Friedman et al., 2002; Liu et al., 2011; Berkelhammer et al., 2012). It is hypothesized that a negative state in these systems (La-Niña, negative PDO, and reverse PNA or RPNA) contributed to alteration of storm tracks delivering precipitation to the region, resulting in drought conditions during the MCA. The relationships between the state of the above mentioned climate modes, moisture source, the isotopic composition of precipitation and the isotopic composition of cave speleothems allowed for this hypothesis to be tested through examination the $\delta^{18}O$ values preserved in LC-1.

CHAPTER 2

BACKGROUND

Geologic Background

Leviathan Cave is located in the Worthington Mountains of central Nevada (~37.8˚N,

115.6˚W) at an elevation of 2110 meters (Figure 2.1). The Worthington Mountains are part of

the Basin and Range geologic province, a series of North/South trending mountain ranges

separated by basins. The formation of the Basin and Range Province, which is typified by horst

and graben topography, is the result of Neogene age east/west extension and extensive normal

faulting (Van Der Pluijm et al., 2004). The Worthington Mountains are composed of Precambrian

and lower Paleozoic carbonate assemblages, upper Paleozoic carbonate and siliceous detrital

formations, and lower Tertiary volcanic formations. Leviathan Cave is located in Devonian

limestone (Crafford, 2007). The cave is located on BLM land within the Worthington National

Wilderness Area and is open to public access. There is little evidence of vandalism within the

cave and the voluntary registry suggests that less than 20 people visit the cave per year. The

designation of the area as a National Wilderness Area prevents any anthropogenic

developments in or above the cave. The cave opening is approximately 40 x 20 m. It is

approximately 220 m down an ~12% grade to the constriction leading to the inner chamber and

approximately 30 m from the constriction to the LC-1 collection site. From this it is estimated

that there is ~100 m of overlying rock above the LC-1 collection site but accurate surveying is

needed to confirm this estimation. The constriction is approximately 1 x 0.5 m. Within the inner

chamber there are active cave drips, cave pools and speleothems. Stalactites and stalagmites up

to ~3-4 m in length are present. Leviathan cave is well above the water table so water emerging

as cave drips originates as precipitation occurring above the cave site and does not include any

contribution from regional aquifers.

Figure 2.1. Digital Elevation Model Map of Central Nevada. Location of Leviathan Cave (37.82˚N, 115.61˚W) is indicated near center of the figure by a red star. Black lines represent highways 375 West, 93 North and 318 North.
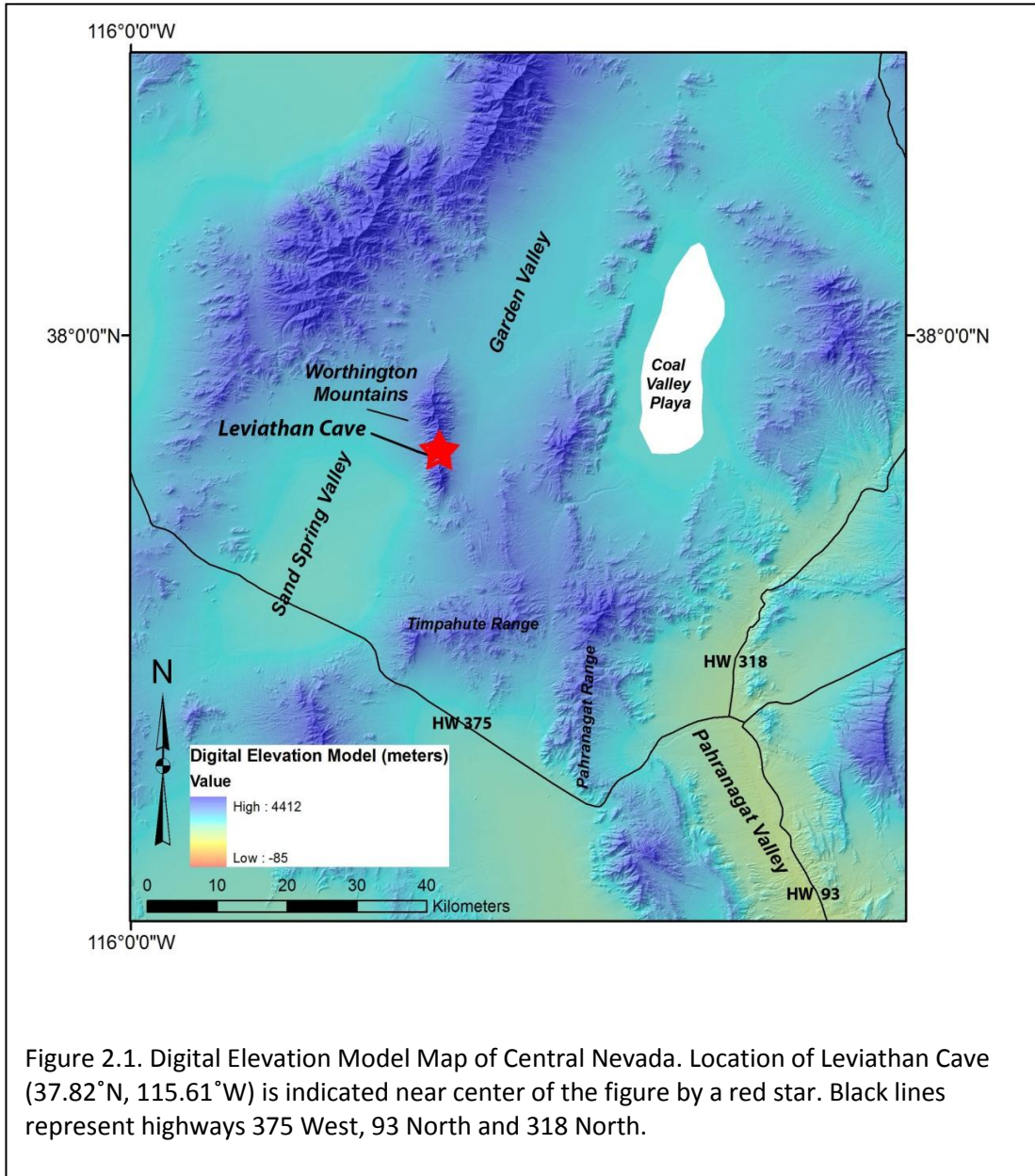
Cave and Speleothem Formation

Limestone caves may provide the suitable environment for speleothem (cave calcite deposits) formation. The suitable conditions for speleothem growth to be used in stable isotope studies include a gradient between the pCO_2 of cave drip waters and atmospheric pCO_2, high relative humidity, low winds, and being under an active drip (Lachniet, 2009). The pCO_2 of the soil overlying the cave is increased above atmospheric levels as a result of respiration from plant roots and oxidation of dead plant material. As rainfall percolates through the soil, CO_2 is absorbed in the form of carbonic acid. When this low-pH water comes in contact with the limestone, calcite is dissolved until reaching saturation. Upon the groundwater emerging in a cave with near atmospheric pCO_2, low pCO_2 results in CO_2 degassing and $CaCO_3$ saturation of drip water. As degassing occurs, solid $CaCO_3$ precipitates leading to the formation of speleothems (Hendy, 1971).

Speleothems are excellent candidates for paleoclimate reconstruction as they can contain information on multiple aspects of the climate system and can be precisely dated using U-series methods (Hendy, 1971; Richards and Dorale, 2003; Lachniet, 2009). Furthermore, speleothems may grow for periods of 10,000 years or more, and it is often possible to achieve decadal and, rarely, annual scale resolution with fine-scale subsampling (Fairchild et al, 2006). Thus, speleothems are able to have a long temporal duration and a high resolution which is often not achievable in other continental paleoclimate proxies, e.g., tree-ring reconstructions or lake sediment records. Another advantage that speleothems have over paleoclimate proxies is that the preservation potential is often higher due to the protective environment of the cave. Surficial proxies may be more prone to having alteration or destruction of the original climate signal through processes such as fire, erosion, bioturbation, reworking of sediment deposits, and

anthropogenic alteration. Speleothems have been shown to be particularly useful for reconstructing processes in the hydrosphere through the examination of oxygen isotopes with the calcite. The oxygen isotope ratios preserved in speleothems can provide information on local to global-scale climate dynamics and resolve forcing mechanisms (Lachniet, 2009).

Oxygen Isotopes

Isotopes of an element contain the same number of protons, but each isotope has a different number of neutrons in the nucleus. Stable isotopes do not decay, but may form from the radiogenic decay of another element. Oxygen exists as three naturally occurring isotopes: ^{16}O, ^{17}O and ^{18}O. Each isotope has 8 protons, and 8, 9, or 10 neutrons. The relative amount of heavier oxygen isotopes is extremely small compared to that of lighter isotopes. Within the ocean and atmosphere 99.759% of oxygen consists of ^{16}O, 0.204% consists of ^{18}O, and the remaining percentage consists of ^{17}O (Sharp, 2007).

Isotope values are reported in delta (δ) notation. Delta notation is the ratio (R=^{18}O/^{16}O) of the heavier isotope (^{18}O) to the lighter isotope (^{16}O) relative to a standard. Delta values are reported in per mil (‰), or parts per thousand. The delta value is defined as

$$\delta = ((R_{sample} - R_{standard})/R_{standard}) \times 1000.$$

The standards for oxygen isotopes are Vienna Standard Mean Ocean Water (VSMOW) for water samples and Vienna PeeDee Belemnite (VPDB) for calcite samples. In this text all $\delta^{18}O$ values will be reported relative to VSMOW and VPDB, respectively.

The ratio between heavy (^{18}O) and light (^{16}O) isotopes can be altered during fractionation processes. Fractionation can be summarized as processes in which one form of an isotope is preferred during a phase change, and the mass of an isotope determines the

likelihood of a particular atom being incorporated into the phase or mineral. Fractionation

occurs during phase changes, from both kinetic effects and equilibrium effects. Kinetic effects

are the result of different translation velocities during phase change as a result of varying mass

(Sharp, 2007). Kinetic fractionation occurs most frequently when relative humidity within the

cave is low and the rate of loss of CO_2 from solution is too rapid for isotopic equilibrium to be

maintained between CO_2 and bicarbonate (Hendy, 1971). Equilibrium effects can be considered

in terms of varying bond energies correlating to different masses. The amount of fractionation

occurring during equilibrium reactions varies as a function of temperature (Sharp, 2007).

Under equilibrium conditions, the $\delta^{18}O$ value in the calcite of a speleothem is a function

of temperature in the precipitated calcite, which should be strongly related to cave air

temperature, and the $\delta^{18}O$ value of the cave drip water from which the stalagmite is formed

(Hendy, 1971). Variation of $\delta^{18}O$ values in speleothem calcite due to variation in cave

temperature is likely to be much smaller than variations due to changes in drip water $\delta^{18}O$

values during the past 2000 years as there is no evidence supporting large scale atmospheric

temperature variation. For example, at an air temperature of ~ 9˚C, each change in temperature

by 1˚C is inversely related to only an ~ 0.22 ‰ change in the $\delta^{18}O$ value of precipitated calcite

(Kim and O'Neil, 1997). In contrast, at a constant temperature each per mil change in the $\delta^{18}O$

value of drip water results in an equal change in precipitated calcite (Kim and O'Neil, 1997; Feng

et al., 2012). In other words, an ~5°C change in cave temperature or one per mil change in the

$\delta^{18}O$ value of cave drip water results to one per mil variation in the $\delta^{18}O$ values of precipitated

calcite.

Kinetic fractionation is most likely to occur in well-ventilated caves with low relative

humidity and low pCO_2. Low relative humidity promotes kinetic fractionation due to evaporation

of cave drip water into the atmosphere, while low atmospheric pCO_2 promotes rapid CO_2

degassing from the drip water (Lachniet, 2009). The larger the gradient between the pCO_2 of

cave drip waters and cave atmosphere, the greater enrichment of ^{18}O in precipitated $CaCO_3$

(Hendy, 1971). To assess the degree in which kinetic fractionation is occurring within a cave one

can test for equilibrium fractionation under modern conditions. To do this, the $\delta^{18}O$ value of

cave drip water, drip temperatures and atmosphere temperatures are measured. Using this

information, calcite $\delta^{18}O$ values precipitated under equilibrium conditions can be predicted,

based on one of several equilibrium fractionation equations, which commonly give contrasting

equilibrium $\delta^{18}O$ values. For this reason, it is appropriate to use the fractionation equation of

Coplen (2007), as it appears to be correct for cave environments (Feng at el., 2012). If the

system is not characterized by equilibrium conditions, kinetic fractionation may obscure part of

the climate signal; yet, studies suggest such stalagmites may still be useable for testing

hypotheses of climate teleconnections (Lachniet, 2009).

The $\delta^{18}O$ value of the cave drip water is the summation of all fractionations that occur

in the hydrologic cycle prior to precipitation passing through the epikarst and emerging as cave

drip water, as well as, any fractionations that occur in the cave environment. Thus, the $\delta^{18}O$

value of drip water is likely to represent multiple precipitation events due to mixing in the soil

and epikarst zones (Lachniet, 2009).

Climate Dynamics and Isotopes in Precipitation

In order to understand the controls on cave drip water, an understanding of modern

climate characteristics is desirable (Lachniet, 2009). The most comparable record of modern

climate conditions for the region comes from Adaven, NV, located ~30 km north of Leviathan

Cave at an elevation of 1914 m (196 m less than Leviathan Cave). From 1914 – 1982 CE, Adaven

received an annual average of 32.4 cm of precipitation, with 60% during the "winter" (Oct.-Mar.)

half of the year and 40% during the "summer" (Apr.-Sept.) half of the year (Figure 2.2). Although

Adaven receives 40% of its precipitation during the summer months, isotopic evidence from the

Great Basin indicates that summer precipitation does not contribute more than ~10% to aquifer

and cave water recharge (Winograd et al., 1998; Prudic and Glancy, 2009).

Figure 2.2. Monthly Averages for Temperature and Precipitation. Monthly averages for temperature (left) and precipitation (right) for the time period 4/1/1914 to 9/28/1982 at Adaven, NV (National Oceanic and Atmospheric Administration. 2004).
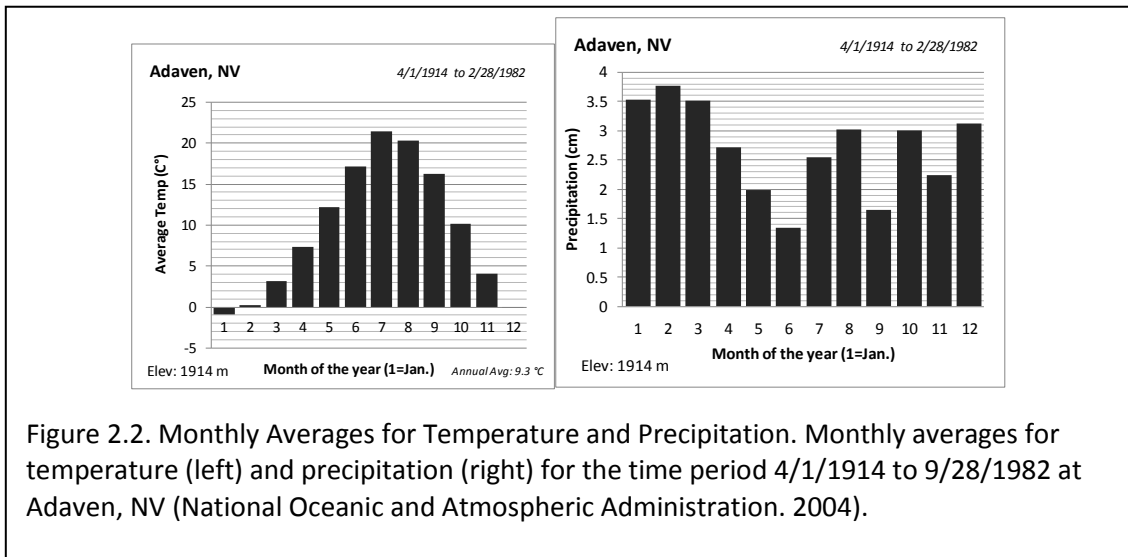
Precipitation events that occur in the region have unique isotopic signatures that are

largely the result of moisture source and are delivered through regional storm tracks (Friedman

et al., 2002; Berkelhammer et al., 2012). Based on precipitation samples from Cedar City, UT,

(~250 km east of Leviathan cave), Friedman et al. (2002), identified 5 groupings of trajectories of

air masses with a distinct range of $\delta^{18}O$ values. Storms originating from the north Pacific had

significantly lower $\delta^{18}O$ values than storms originating from the tropical Pacific, the Gulf of

California, and the Gulf of Mexico (Friedman et al., 2002). Analysis of five years of isotopic

measurements of precipitation, from 4 locations in southern California, also resulted in the

conclusion that in the western US, the dominant control on the isotope values of winter

precipitation is varying atmospheric moisture source between high and low latitudes. Storms

originating from high latitudes have significantly lower $\delta^{18}O$ values than storms originating from

low latitudes (Berkelhammer et al., 2012). Similar results were obtained by Friedman et al.

(2002) who observed moisture originating from the North Pacific had an annual average $\delta^{18}O$

value of ~-14.2 ‰, with values ranging from ~-24 ‰ to ~-8 ‰. Storms from the tropical Pacific

had an annual average $\delta^{18}O$ of ~-11.8 ‰, with values ranging from ~- 26 ‰ to ~-4 ‰ (Friedman

et al., 2002).

Modes of Pacific Climate Variability

Pacific Basin circulations and North American climate are connected through

atmospheric teleconnections. Three important modes of variability in the Pacific Basin and

North America are El Niño/Southern Oscillation (ENSO), the Pacific Decadal Oscillation (PDO)

and the Pacific North American (PNA) teleconnection. ENSO, which contains the extremes of El

Niño and La Niña, has a particularly strong influence on precipitation occurrence and

distribution in North America making it capable of generating abrupt changes in weather

patterns (Ropelewski and Halpert, 1986; Kurtzman and Scanlon, 2007). There is an observed 2-8

year periodicity observed in the ENSO system (Kurtzman and Scanlon, 2007). El Niño (warm

phase) events are characterized by weakening of the tropical easterly trade winds and

displacement of atmospheric low pressure zones to the central tropical Pacific Ocean. This

process results in increased sea surface temperatures in the central and eastern tropical Pacific,

which is accompanied by decreased atmospheric pressures across southwestern North America.

La Niña (cool phase) events occur when the easterly trade winds are particularly strong which

results in an increase of cold water upwelling along the equatorial eastern Pacific Ocean. This is

accompanied by increased atmospheric pressure in the southwestern United States (National

Oceanic and Atmospheric Administration, 2005). La Niña (El Niño) is associated with decreased

(increased) precipitation occurrence in southwestern North America (Ropelewski and Halpert, 1986; Cole et al., 2002). The El Niño and La Niña phases of ENSO have also been associated with a change in moisture origin latitude for precipitation reaching the Great Basin. The El Niño (La Niña) phase is associated with increased storms originating from low (high) latitudes. This results from the displacement of the Pacific jet stream and associated storm tracks. El Niño occurrence strengthens the jet stream over the low latitude Pacific. In contrast, La Niña creates a more variable Pacific jet stream and strengthens the Polar jet stream (National Oceanic and Atmospheric Administration, 2009).

The Pacific Decadal Oscillation (PDO) is a pattern of north Pacific variability which can have an influence on climate in North America (Mantua and Hare, 2002). The PDO is characterized by decadal-scale variance of sea surface temperature (SST) along the north-western coast of North America. The PDO warm (cool) phase is characterized by increased (decreased) sea surface temperatures along the Pacific coast of western North America, and cooler sea surface temperatures in the north-central Pacific (Mantua and Hare, 2002). The PDO has also been shown to alter precipitation patterns over western North America. PDO fluctuations are most energetic on 15-20 and 50-70 year intervals (Mantua and Hare, 2002), but PDO variability is partially dependent on ENSO at all time scales (Newman et al., 2003). For this reason more attention has been given to ENSO. Similar to ENSO, the warm (cool) phase of PDO has been correlated to increased (decreased) winter precipitation in the southwest region of North America (Kurtzman and Scanlon, 2007). The PDO has also been shown to modulate ENSO effects on precipitation in North America (Kurtzman and Scanlon, 2007); i.e., the strength of the ENSO/PDO may be amplified or diminished due to interference between the PDO and ENSO (Biondi et al., 2001).

The Pacific North American (PNA) teleconnection is a dominant mode of atmospheric circulation over the Pacific Ocean and North America (Leathers et al., 1991; Yin, 1994; Trouet and Taylor, 2009; Liu et al., 2011). The mean atmospheric flow over North America and the Pacific is characterized by a trough and ridges in Rossby waves. There is a trough over the east-central North Pacific and eastern North America, while there is a ridge over the northern Rocky Mountains. The PNA index represents the strength and mode of the PNA. The PNA index is calculated using the 500-mb or 700-mb height at the nearest weather station (47.9°N, 170.0°W; 49.0°,111.0°W; and 29.7°N,86.3°W) to the center of action for the Rossby wave trough and ridges (Yarnal and Diaz, 1986; Leathers et al., 1991). The PNA index is constructed so that the meridional extreme corresponds to positive values, while the zonal corresponds to negative values. The positive, or meridonal, phase (PPNA) represents a more north-south character of 700-mb flow while the negative (reverse), or zonal, phase (RPNA) represents a more east-west character (Figure 2.3; Leathers et al., 1991).

Figure 2.3. Character of 700-mb flow during PNA phases. Zonal flow is the negative state (RPNA) and Meridional flow is the positive state (PPNA). Figure after Leathers et al. (1991).
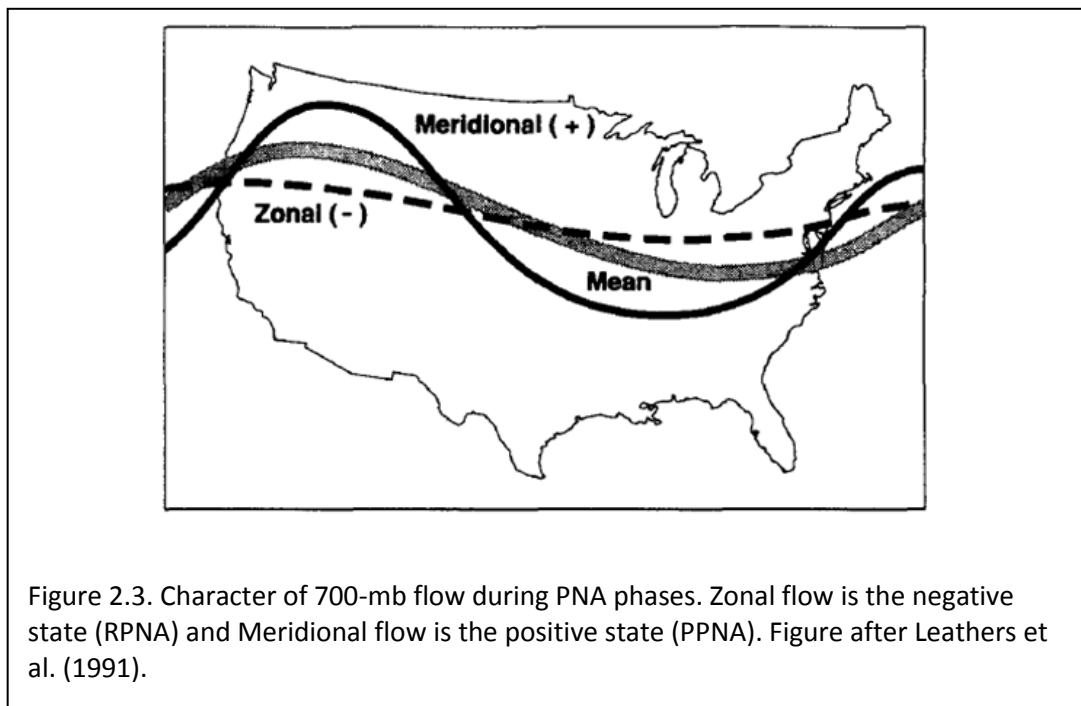
The phases of the PNA have the greatest influence on atmospheric circulation across

North America during December and January (Blackmon et al., 1984). Under PPNA conditions a

blocking high pressure ridge is present over western North America which results in the

deflection of Pacific storm tracks along a more meridional south-to-north track. The PPNA is

thus associated with more southerly moisture source. The opposite response is seen during

RPNA. In the southwestern USA, correlation between the PNA phase and precipitation amount

or temperature is relatively weak compared to the northwestern, USA (Leathers et al., 1991; Yin,

1994). Yet, rearrangement of winter storm tracks results in changes of the δ^{18}O value of

precipitation by the processes described in the studies of Friedman et al. (2002), and

Berkelhammer et al. (2012). Recent work by Liu et al. (2011), demonstrated that this

rearrangement results in correlation of δ^{18}O values of precipitation and the PNA index across

the contiguous USA. The strongest correlation between the δ^{18}O of precipitation and PNA phase

was observed in the southwest U.S. at Flagstaff, AZ, on the Colorado Plateau just downwind of

the Great Basin. A positive correlation was observed between δ^{18}O values in precipitation and

PNA phase resulting from moisture transport variations associated with each phase (Figure 2.4).

When a PPNA configuration is present, δ^{18}O values are higher in precipitation because of a more

southerly moisture source, and vice-versa for the RPNA configuration (Liu et al., 2011).

ENSO, PDO and PNA do not behave entirely independently and are capable of enhancing

(diminishing) the effects of each other when they are in (out of) phase. For example, ENSO and

PDO can modulate the frequency and strength of the PNA pattern (Trouet and Taylor, 2009).

ENSO and PDO alter storm track distribution in similar spatial patterns as the PNA phases, and

the resulting changes in moisture source can largely be accounted for through observation of

PNA circulation patterns (Liu et al., 2011). It is possible to isolate the PNA phase in

reconstructions by using multiple, correlated records from western and midwestern North

America, but a reconstruction of PNA from a single location would be the integrated expression

of the three modes expressed as the modulation of the PNA (Liu et al., 2011).

Figure 2.4. Correlation of $\delta^{18}O$ values in precipitation and PNA phase. $\delta^{18}O$ values of precipitation collected at Flagstaff, AZ, on the Colorado Plateau just east of the Great Basin plotted against PNA index. Figure after Liu et al. (2011).
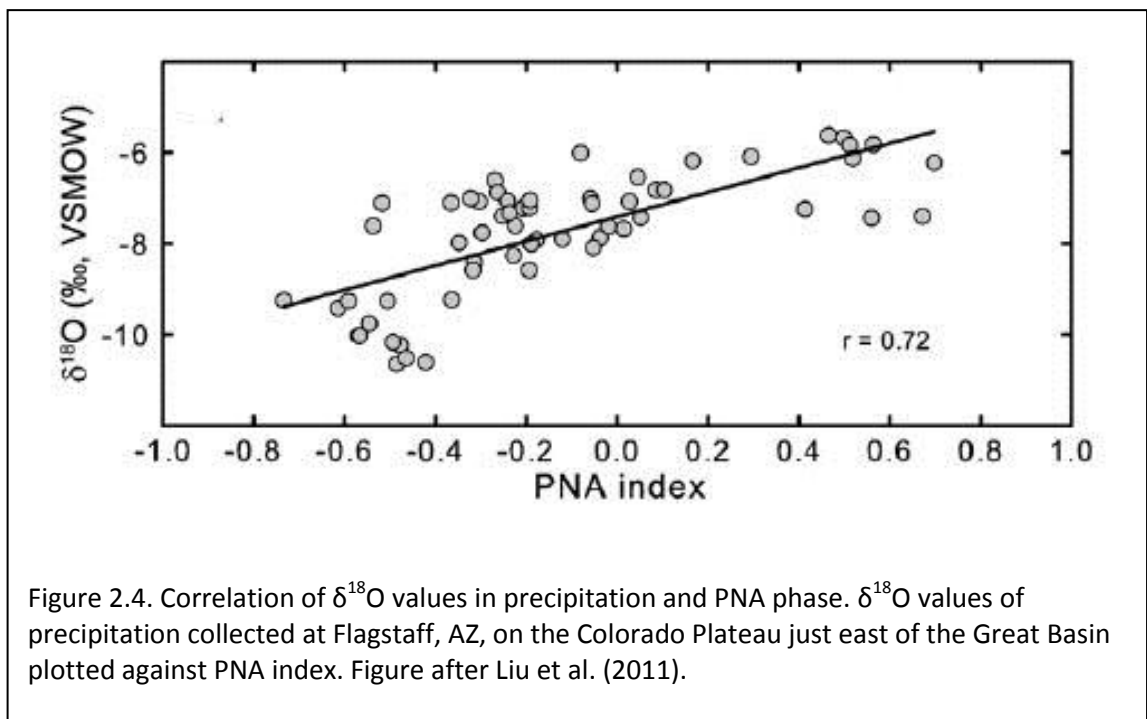
$^{238}U - ^{234}U - ^{230}Th$ Dating Techniques

Application of the ^{238}U-^{234}U-^{230}Th method requires processes to preferentially

incorporate uranium over thorium in the $CaCO_3$ of a speleothem such that it creates a

disequilibrium state and the decay chain "clock" begins at zero. This process occurs largely in the

hydrosphere and waters from which terrestrial carbonates are formed. Uranium is readily

mobilized, particularly as the uranyl ion UO_2^{2+} and its complexes, resulting in uranium sorption

to organic matter (Richards and Dorale, 2003). Thorium concentrations in terrestrial waters are

often much lower than those of uranium due to the low solubility of ThO_2 and strong sorption

properties (Porcelli and Swarzenski, 2003). Although, the uranium and thorium concentrations

in meteoric water are controlled by ionization potential, pH, source rock mineral composition

and water rock interaction time (Richards and Dorale, 2003). Uranium and thorium abundances

in deposits precipitated from solution generally reflect abundance in the hydrosphere. Due to

processes in the hydrosphere, as well as difference in atomic size, there generally is a near

absence of thorium and the preferred inclusion of uranium in the co-precipitated $CaCO_3$

(Richards and Dorale, 2003).

Material used for U-series dating should be primary and unaltered, this helps ensure

that the speleothem has behaved as a closed system (Richards and Dorale, 2003). Secondary

mineralization may allow for contamination to occur. Sub-samples of speleothem calcite can be

obtained using a micro-drill and preferably contain the fewest number of growth layers possible.

This helps to ensure accurate dating as initial uranium concentration in the water from which

they form may not be constant throughout the growth of the speleothem.

The dating process begins by first powdering the carbonate sample, which is then

dissolved in HNO_3, and spiked with a mixed solution of ^{229}Th-^{233}U-^{236}U. Spiking the sample with

known concentrations of non-radiogenic isotope, allows the ratios of radiogenic isotopes to be

determined. Uranium and thorium are then co-precipitated with pure $FeOH_3$ and subsequently

separated. Isotopic ratios are then measured with a multi-collector ICP-MS (Polyak and Asmerom, 2001).

Ages are derived from the measured ratios of $^{235}U/^{233}U$, $^{234}U/^{235}U$, $^{230}Th/^{229}Th$, and $^{232}Th/^{229}Th$. These measurements allow for the calculation of $^{232}Th/^{238}U$, $^{230}Th/^{238}U$ and $^{230}Th/^{234}U$ ratios which are related to decay rates. Accurate decay constants, and half-life determinations, are necessary for correct age calculations. The most accurate half-life for ^{238}U is $4.4683 \pm 0.0024 \times 10^{9}$ years (Jaffey et al., 1971). The half-life for ^{234}U is $245,250 \pm 490$ years and the half-life for ^{230}Th is $75,690 \pm 230$ years (Cheng et al., 2000). All errors reported are 2σ.

Calculated ages must be corrected for any initial daughter products. Correcting for initial ^{230}Th requires an estimate of the initial $^{230}Th/^{232}Th$ ratio. If ^{232}Th contamination is low, the effect of using an incorrect initial $^{230}Th/^{232}Th$ ratio is negligible (Richards and Dorale, 2003). It is possible to thoroughly check for initial ^{230}Th contamination using total dissolution (as outlined above) and isochron methodology (Richards and Dorale, 2003). The construction of isochrons in speleothems requires two or more sub-samples from coeval $CaCO_3$ material. Plotting the $^{238}U/^{230}Th$ ratios will reveal if the speleothem has behaved as a closed system and if it is a two component system, as well as, allow for calculation of initial $^{230}Th/^{232}Th$ ratios (Richards and Dorale, 2003). When isochron techniques are not applied, an initial $^{230}Th/^{232}Th$ ratio of 4.4×10^{-6} assuming a silicate component with the Bulk Silicate Earth $^{232}Th/^{238}U$ ratio of 3.8 may be used (Polyak and Asmerom, 2001; Lachniet et al., 2004). Additionally, regression of isotope data from three or more coeval samples provides robust results, but requires confidence in identifying coeval material (Richards and Dorale, 2003). This can be particularly useful in speleothem analysis where detrital contamination may vary across growth layers due to differences in energy of fluid flow and a single sample may give misleading results. Variation in detrital

contamination across the surface is a concern, and thus samples collected along the growth axis are preferable because the high energy of drip impact minimizes detrital contamination (Richards and Dorale, 2003).

Ages obtained from U-series methods should be consistent stratigraphically within the deposit. Ages that do not agree stratigraphically suggest secondary alteration or recrystallization, older detrital contamination of younger $CaCO_3$ or contamination of the sample during preparation or analysis. Multiple ages from material precipitated during the same interval, such as along a growth band, should be in agreement (Richards and Dorale, 2003). Detection of growth hiatuses can be done through examination of speleothem $CaCO_3$ fabric or may be indicated by large jumps in dates over small distances/depths of the speleothem material. A growth hiatus may indicate conditions in the cave were not favorable for speleothem formation or that the drip migrated away from the speleothem. Growth rates may vary through time due to changing climatic conditions and/or changes in conditions within the cave (Fairchild et al., 2006).

The number of sub-samples and dates generated from a speleothem needed for an accurate age model varies with application. In general, the quality of the age model increases with an increasing number of samples. Interpolation and extrapolation from calculated dates has been approached in several ways. Linear regression, linear interpolation, polynomial fits and smoothing splines can be used to define the most likely age versus depth relationships (Richards and Dorale, 2003). Techniques of interpolation or extrapolation are not trivial, particularly if the data is to be used for frequency analysis (Richards and Dorale, 2003). If modern cave conditions are favorable for speleothem growth and the speleothem is collected from under an active drip

there is justification for assigning a zero age to the tip of the speleothem when generating an age model.

Previous Paleoclimate Reconstructions

Of the past two thousand years, the interval from ~900-1350 CE, widely known as the Medieval Climatic Anomaly (MCA), has been the target of much research. The first paleoclimatic observations uniquely describing this time interval, referred to as the Medieval Warm Epoch (Lamb, 1965), was based on historical accounts and western Europe paleoclimate data. It was concluded European temperatures were elevated and winters mild around the dates 1100 to 1200 CE (Lamb, 1965). Because this time interval was also associated with hydrologic anomalies observed in other regions, it more appropriately referred to as the Medieval Climatic Anomaly or MCA (Stine, 1994).

A multitude of paleoclimate reconstructions show anomalies during the MCA. Summarized in Mann et al. (1999) it appears during the past 1000 years, Northern hemisphere temperatures were the highest during 20th century and temperatures were higher during MCA than the time between the MCA and the 20th century. Additional work has shown that temperature and other climatic anomalies varied regionally (Hughes and Diaz, 1994; Mann et al., 1998; Mann et al., 1999; Jones and Mann, 2004). If warmer temperatures were contributing to development of other climate anomalies, then investigation of associated climate behavior may be useful in predicting future climate variation induced by anthropogenic warming. However, because greenhouse gas concentrations were far below modern level during the MCA, the time interval cannot be used as a direct analog to modern or future conditions, but rather shows the potential climate variability associated with pre-industrial CO_2 concentrations, and is thus useful end-member for evaluating future climate change at higher CO_2 concentrations.

A reconstruction from Mono Lake, CA, located on the eastern flank of the Sierra Nevada indicates drought conditions were particularly persistent during the MCA (Stine, 1990). This is consistent with the reconstructed flow of the Merced River in the same drainage as Mono Lake (Graham and Hughes, 2007). The Lake Tahoe basin also experienced drought during the MCA, indicated by submerged trees located on paleoshorelines established during lake regression driven by increased aridity (Kleppe et al., 2011). Drought reconstructions generated from tree rings in the Sierra Nevada also indicate decreased precipitation conditions during the MCA (Cook et al., 2004; Cook et al., 2007).

Previous work in the Great Basin supports anomalous climate during the MCA, but climate signals vary geographically. Dendroclimatic reconstructions from the central Great Basin indicate greater incidence of persistent drought between 400 – 1500 CE, but there is a greater indication that drought occurred in the western portion than in the eastern portion of the central Great Basin (Hughes and Funkhouser, 1998). Stella Lake in the central Great Basin showed a muted response to increased aridity during the interval 900 – 1100 CE (Reinemann et al., 2009). Although, with the sampling interval of 100 years and ^{14}C chronology uncertainties, it's difficult to assign ages to identify the MCA interval and conclude if there was an anomalous climatic response at this locale (Reinemann et al., 2009).

Several pollen ratio-based reconstructions, including Newark Valley pond (Smith, 2003) and Kingston Meadow (Mensing et al., 2006), from central Nevada have been interpreted to indicate wetter than average conditions during the MCA. This occurred at the same time that the eastern Sierra Nevada was in a period of drought (Mensing et al., 2008). Although, Mensing et al. (2008), acknowledge that the data from the Nevada lakes is difficult to interpret and may be misleading as the resolution of these records does not allow for clear identification of events on the century scale. The inability to discern less than century scale events in these records is

due to low sedimentation rates resulting in low temporal resolution at the sampling interval. At

Newark Valley pond sample resolution is ~244 years, and at Kingston Meadow sample

resolution is ~260 years. A hiatus of unknown age and duration is observed in the Kingston

Meadow record contributing to the difficulty of establishing a reliable age model (Mensing et al.,

2008). Pollen ratios in sediments from Diamond Pond in southern Oregon, which has sufficient

resolution to discern decadal scale events, indicates there was increased moisture during this

time and appears to fall in a region beyond the northern extent of the drought terminating at

1200 CE (Mensing et al., 2008). At Lower Pahranagat Lake (~100 km south of Leviathan cave) a

decrease in the conifer-to-saltbrush pollen ratio within the sediments has been interpreted as

an indicator of drier conditions between 300-500 CE and an extended dry MCA period from 800-

1450 CE (Wigand, 1997).

Additionally, increased fire occurrence is often linked to increased aridity in mountain

regions. Beaty and Taylor (2009) have shown that charcoal sediments preserved in lakes and

meadows of the Sierra Nevada region indicate increased fire occurrence during the MCA

compared to the following 1000 years.

Paleoclimatic Reconstruction of Pacific Climate Variability

The three primary modes of Pacific climate variability that have an impact on the

southern Great Basin region are ENSO, PDO and PNA. Thus, reconstruction of the state of these

modes during the MCA can help attribute causality of observed anomalies in regional

paleoclimate records. Instrumental records of ENSO, PDO and PNA have insufficiently-long

durations with which to investigate centennial-scale changes. To analyze the state of these

phenomena on longer time scales, proxy records must be used to establish reconstructions. A

variety of proxy records have been used to approach this problem for ENSO, although many of

these reconstructions provide contradictory results. Long-lived corals and fossil corals from the

tropical Pacific have provided high-resolution paleoclimate reconstructions of ENSO. Analysis of

$\delta^{18}O$ values of overlapping fossil coral segments from Palmyra Island in the Tropical Pacific

suggests that La Niña-like conditions were generally present during at least short interval within

the MCA (Cobb et al., 2003). Terrestrial records can complement oceanic coral records. El Niño

frequency reconstructions from the Galapagos and Ecuador, based on lake sedimentation

characteristics, show a general increase in El Niño events during the MCA (Moy et al., 2002;

Conroy et al., 2008). Speleothems have also been used with success in reconstructing ENSO

occurrence. Lachniet et al. (2004) suggested that $\delta^{18}O$ values of a speleothem collected in

Panama indicated increased dry conditions from 1100-1200 CE, which was attributed to an El

Niño forcing. In contrast to the Ecuador, Galapagos, and Panama records, analysis of spatial

precipitation patterns during the MCA, combined with modeling results, have been used to

conclude that observed drought conditions in North America could be attributed to the tropical

Pacific being in an extended La Niña-like state (Cook et al., 2007). These conflicting results

demonstrate that there is still much work to be done before a solid conclusion can be agreed on

concerning the state of ENSO during the MCA.

Reconstruction of the PDO comes from both instrumental and proxy records.

Instrumental records have been used to reconstruct the PDO for the time period of ~ 1900 CE to

present (Mantua et al., 1997). A PDO reconstruction created through the calibration of tree-

rings in PDO sensitive regions to the instrumental record indicates a strong negative PDO state

from 900-1300 CE (MacDonald and Case, 2005).

Instrumental records of the PNA mode have only been available since the 1950's when

mid-troposphere measurements became common. This record is too short to evaluate long-

term dynamics and variability of the PNA phenomenon (Trouet and Taylor, 2009). There are very few paleoclimate reconstructions extending the record of PNA beyond the instrumental record. The strong influence of PNA on climate in North America and the possibility that PNA-like shifts may have occurred during the MCA prompts further research in this area (Liu et al., 2011). Two reconstructions that extend the PNA index beyond the instrumental record have been presented in work by Yin (1994), and Trouet and Taylor (2009). Yin (1994) extended a PNA reconstruction from 1947 to 1895 using a regression model based on the relationship of the PNA index and the temperature anomaly field across the continental United States. A rather weak but significant correlation has been found between the PNA and SO indices suggesting shared variance between the PNA and ENSO systems (Yin, 1994). Twelve tree ring width chronologies were selected from the core region of PNA influence on winter climate were used to create a reconstruction which extends to 1700 CE (Trouet and Taylor, 2009). The reconstruction by Trouet and Taylor (2009) revealed that the PNA was in a negative phase at 1700 before rising to a positive phase at ~1815 CE. Following ca. 1815, PNA index drops to negative phase from ~1840-1950 CE. From 1950 CE to present the PNA phase has increasing (Trouet and Taylor, 2009). Currently no proxy reconstructions of the state of the PNA system and associated climatic responses for western North America during the MCA have been presented in peer reviewed literature. A proper proxy for reconstruction of the PNA should be most sensitive to winter climatic conditions, as this is the time when the PNA is most energetic, and should record atmospheric circulation variations, such as changing moisture sources or anomalous temperature fields, which have been correlated to changes in the PNA system (Liu et al., 2011).

CHAPTER 3

METHODS

Sample Collection and Preparation

The sampled speleothem (LC-1) was collected from Leviathan Cave on April 23, 2011

(Figure 3.1). The stalagmite LC-1 measured 56 cm along its growth axis and had a circumference

of ~33 cm along the base and ~16 cm one cm below the tip. LC-1 was located approximately 50

m to the NE of the constriction into the inner chamber. LC-1 was chosen because it was located

in the area of highest relative humidity and minimal ventilation, which increased the likelihood

the speleothem was suitable for stable isotope studies (Lachniet, 2009). To confirm the location

within the cave exhibited the proper conditions, relative humidity and temperature were

monitored with a HOBO® data logger left in the cave from 5/27/2011 to 6/2/2012.

Measurements were taken every 2 hours. The accuracy of the data logger is ± 0.21°C for

temperature and ± 2.5% for relative humidity. To ensure that sample removal would have

minimal aesthetic impact and minimal environmental effects, sample selection was approved by

a BLM agent and the chairman and members of the National Speleological Society (NSS),

Southern Nevada Grotto (SNG). Approval of sample selection by these entities (BLM and NSS)

helps ensure cave conservation and regulates the legality of speleothem collection. Sampling

was performed under the Bureau of Land Management permit # 8560.
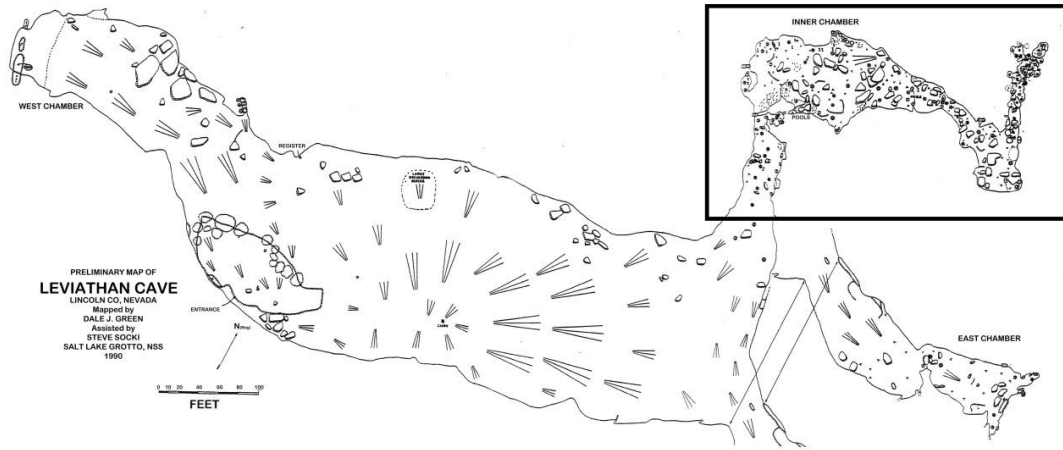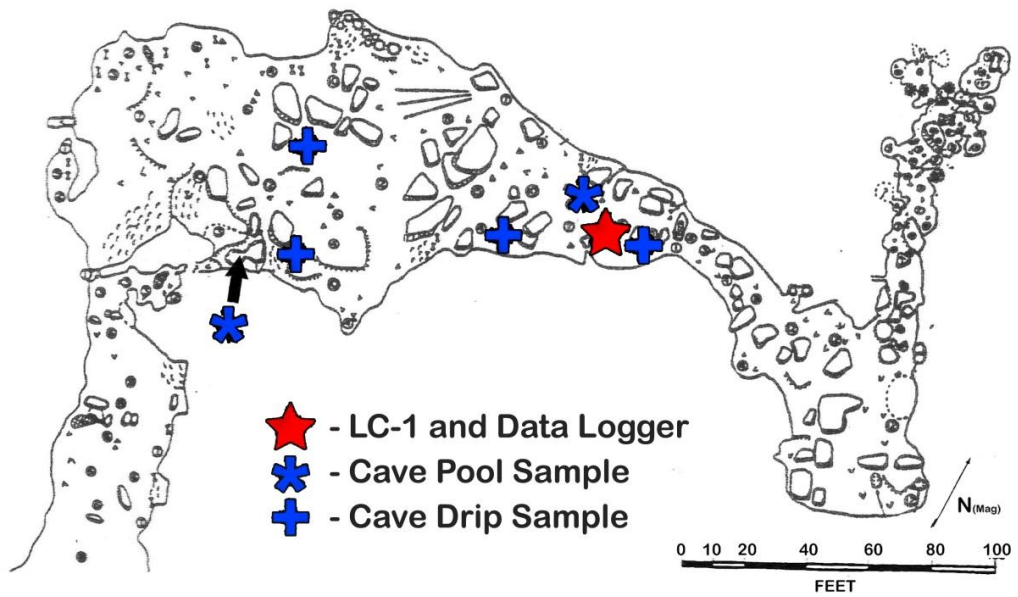
Figure 3.1. Leviathan Cave map and sampling locations. Top shows the complete Leviathan cave map; inset (rectangle) shoes location of detail (bottom). Locations of cave data logger and sampling locations are shown. Values for water samples are reported in Table 1. Map from Dave Green, Salt Lake Grotto, NSS, 1999.

LC-1 was halved along the approximate growth axis using a circular saw. The halves were then slabbed to a thickness of ~2 cm, resulting in slabs mirrored across the growth axis. One half was preserved as an archive and will remain in storage at UNLV in the Las Vegas Isotope Science (LVIS) Laboratory. The other half was polished by hand to reveal the growth layers and to elicit growth axis orientation which determined location of stable isotope sampling. The polished half was photographed before further work proceeded.

Radiometric Dating

Radiometric dating procedures and analysis was conducted by the University of New Mexico Radiogenic Laboratory. Ten calcite samples of ~0.08 to 0 .20 g were drilled parallel to growth laminae and along approximate growth bands from the top 84 mm of LC-1. The chemical purification and separation of uranium and thorium was conducted according to procedures outlined by Polyak and Asmerom (2001). U-series analysis ages are reported with uncertainties of 2σ of the mean. The global initial ^{230}Th/^{232}Th value of 4.4 x 10^6 with an uncertainty of ± 50 % was used for age calculation. An age model was created by setting the tip of the stalagmite to zero age (because LC-1 was collected under an active drip) and then linearly interpolating between obtained dates. Ages were assigned to stable isotope analysis depths by linear interpolation.

Stable Isotope Sampling

LC-1 was subsampled for analysis of the oxygen isotope ratios. Subsamples were obtained from the cut and polished half using a Sherline model 5410 mill equipped with a digital readout of bit position and a 0.5 mm-diameter bit to ensure sampling accuracy. A sampling interval of 0.1 mm was achieved by continuous micromilling at an ~1 mm depth from the tip of the growth axis towards the base. This process generated 841 calcite subsamples of ~200 μg

from the top 84.1 mm of the speleothem. Every sample was analyzed for the top 16.5 mm, after which every other sample was analyzed, for a total of 498 samples. This was done because there was not significant variation between the $\delta^{18}O$ values of each 0.1 mm sample. All subsamples were analyzed with a Kiel IV automated carbonate preparation device directly coupled to a ThermoElement Delta V plus mass spectrometer at the Las Vegas Isotope Science (LVIS) Lab at the University of Nevada, Las Vegas. Precision was better than 0.08 ‰.

Water Samples

Water samples were collected from within the cave in the form of cave drip water and cave pool water (Figure 3.1). Sample NV-11-04 was collected on from a small drip water pool and samples NV-11-05 and NV-11-06 were collected from active drips near the LC-1 collection site within Leviathan Cave. Sample NV-11-05 was later discarded due to air headspace in the vial, which could have altered the $\delta^{18}O$ value because of evaporation.

Water samples were also collected from nearby lakes and springs. Sample NV-11-01 was collected at the shore (~0.5 m water depth) of Lower Pahranagat Lake (37.23° N, 115.08° W). Samples NV-11-02 and NV-11-08 were collected from a ground water source at Ash Springs (37.46°N, 115.19°W). Samples NV-11-03 and NV-11-07 were collected at the head of Crystal Spring (37.53° N, 115.23° W). Samples NV-11-01 through NV-11-06 were collected on April 22nd and 23rd, 2011. Samples NV-11-07, taken from the Crystal Springs head, and NV-11-08, taken from the Ash Springs head, were collected on September 5th, 2011.

All water samples were analyzed with a ThermoElectron TC/EA device directly coupled to a ThermoElectron Delta V plus mass spectrometer at the Las Vegas Isotope Science (LVIS) Lab at the University of Nevada, Las Vegas. Internal standards were calibrated with international

standards on a scale where values of SLAP are defined as -55.5 and -428 ‰ for δ^{18}O and δD, respectively. Values are reported relative to VSMOW. Precision was better than 0.15 ‰.

Statistical Analysis

Spectral analysis was conducted using the program REDFIT (Schulz and Mudelsee, 2002). This allowed for the estimation of red-noise spectra directly from the unevenly spaced δ^{18}O time series without the need of time interpolation. This prevented a bias for low-frequency components at the cost of high-frequency components which results from interpolation (Schulz and Mudelsee, 2002).

Wavelet transformation was also conducted to determine the periodicity of δ^{18}O variation, and how the periodicities changed over time which was not accomplished through spectral analysis (Torrence and Compo, 1998). In order to perform wavelet analysis the stable isotope time series was statistically subsampled with linear interpolation at 4 year time steps. This interval was chosen as it was close to the true average sampling resolution. Choosing an interval close to the average sampling interval for interpolation avoids both aliasing and oversampling. For wavelet analysis, the interpolated time series was detrended by subtracting the linear trend from the original time series. Values were also normalized to standard deviation units. Wavelet analysis was conducted on the detrended time series in a MatLab script using a Morlet wavelet with a wave number of 6.

CHAPTER 4

RESULTS AND INTERPRETATION

Cave Environment and Water Samples

Eight water samples were collected and analyzed for isotopic composition from within

Leviathan Cave and from surface and spring waters near the study site. The δ^{18}O and δD values

of water samples are reported in Table 1. The δ^{18}O values of cave drip water and cave pool

water are, respectively, -14.2 ‰ and -14.0 ‰. These values are similar to nearby spring waters

which have values ranging from -14.8 ‰ to -15.0 ‰. The difference between the spring and

cave waters is attributed to the fact spring waters are sourced from the regional aquifer and the

cave waters are not, representing local precipitation recharge to the cave system instead. The

only lake water sample collected exhibited a δ^{18}O value of -8.8 ‰. This sample is interpreted to

have significant evaporative enrichment due to high evaporation rates in the region and near

surface sample collection because the isotopic values fall below the meteoric water line in the

evaporative enrichment field.

Sample ID	Description	Longitude	Latitude	Altitude	Type	Date	Time	δD (‰ SMOW)	δ^{18}O (‰ SMOW)	d-excess
NV-11-01	Lower Pahranagat Lake	-115.08468	37.22587	973.0	Lake	4/22/2011	14:00	-82	-8.8	-12.2
NV-11-02	Ash Springs	-115.19436	37.46319	1093.0	Spring	4/22/2011	14:30	-112	-14.8	6.2
NV-11-03	Crystal Spring Head	-115.23375	37.53191	1156.0	Spring	4/22/2011	15:00	-113	-15.1	7.7
NV-11-04	Leviathan Cave Pool	-115.60642	37.82949	2404.0	Cave Pool	4/23/2011	12:30	-104	-14.0	8.8
NV-11-05	Drip by pool, Leviathan Cave	-115.60642	37.82949	2404.0	Drip	4/23/2011	12:30	DISCARDED DUE TO HEADSPACE		
NV-11-06	Drip by pool, Leviathan Cave	-115.60642	37.82949	2404.0	Drip	4/23/2011	12:30	-105	-14.2	9.2
NV-11-07	Crystal Springs	-115.23375	37.53191	1156.0	Spring	9/5/2011	NA	-112	-15.2	9.5
NV-11-08	Ash Springs	-115.19436	37.53191	1156.0	Spring	9/5/2011	NA	-112	-15.0	7.9

Table 1. Stable Isotope Values of Water Samples. List includes cave pools, cave drips, springs, and lake water samples.

The δ^{18}O values of the cave drip water are interpreted to be the representative of the

average δ^{18}O value of winter precipitation. This inference is supported by isotopic evidence that

as much as 90% of spring and cave water recharge comes from winter precipitation in nearby

regions of the Great Basin (Winograd et al., 1998; Prudic and Glancy, 2009). Stronger evidence

for this inference comes from the observation that the $\delta^{18}O$ values observed in cave drip waters

at Leviathan cave are in the range of winter precipitation values (~-18 ‰ to -12 ‰) observed by

Friedman et al. (2002) and Berkelhammer et al. (2012), in contrast to the range of summer

precipitation values (~-10 ‰ to +8 ‰). Additionally, cave water samples fall on the meteoric

water line for the region and do not fall in the evaporative enrichment field (in contrast to water

sample NV-11-01) suggesting that waters contributing to cave drip waters do not undergo

significant evaporative enrichment, which is assumed to occur in summer precipitation (Figure

4.1).

Figure 4.1. Meteoric Water Lines and Water Samples. Water samples from drips and pools within Leviathan cave indicated by crosses. Global Meteoric Water Line indicated by GMWL. LMWL from Friedman et al. (2002) for Cedar City, Utah.
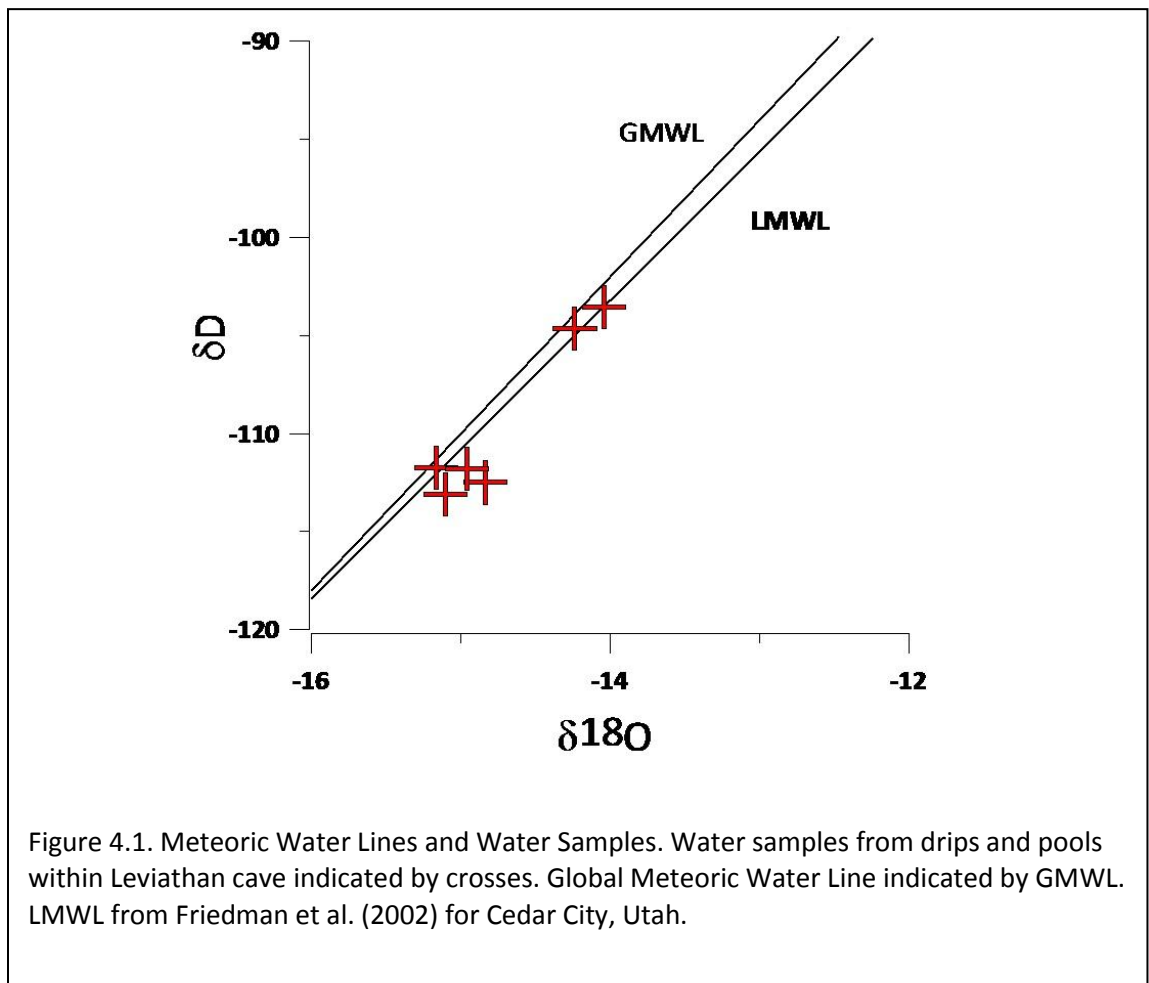
The data logger left in the cave indicated that relative humidity was consistently near 100% and cave temperature was consistent at 8.27°C ± 0.03. This indicates that the atmosphere is very stable and consistent and is the proper environment to promote equilibrium fractionation over kinetic fractionation as relative humidity is high and temperatures do not fluctuate (Lachniet, 2009).

Geochronology

Ten dates were obtained from the upper 84 mm of LC-1 representing 2095 years of growth (Table 3). Growth rates vary from 0.02 mm/yr in the most recent 6.5 mm of growth (317 years) to 0.09 mm/yr between 22.5 and 26.5 mm (~1270-1277 CE). The average growth rate was ~ 0.042 mm/yr. The tip was set to zero age because the sample was collected under an active drip. There are no periods which indicated growth hiatuses in the upper 84 mm of LC-1 (the past ~2095 years of growth). All of the dates were in correct stratigraphic order except for the date obtained from growth bands 43 mm from the tip. This date was removed from the age model, because its high ^{232}Th ratios indicate silicate detrital contamination with anomalous ^{230}Th/^{232}Th ratios. In all other samples uncertainty is less than ± 20 years. Ages were assigned to δ^{18}O values by linearly interpolating between U-series dates (Figure 4.2).

Depth (mm)	^{238}U (ng/g)	^{232}Th (pg/g)	^{230}Th/^{232}Th activity ratio	^{230}Th/^{238}U activity ratio	Measured δ^{234}U (‰)	Initial δ^{234}U (‰)	Uncorrected age (yr BP)	Corrected age (yr BP)
7	362 ± 0.33	696 ± 23	16 ± 1	0.0006291 ± 0.0000208	2226 ± 3	2228 ± 3	335 ± 7	317 ± 11
14	340 ± 0.28	584 ± 38	27 ± 2	0.0005616 ± 0.0000362	2213 ± 3	2216 ± 3	507 ± 11	491 ± 13
23	339 ± 0.21	710 ± 57	32 ± 3	0.0006865 ± 0.0000549	2190 ± 3	2195 ± 3	757 ± 17	738 ± 19
27	358 ± 0.19	488 ± 30	51 ± 3	0.0004456 ± 0.0000272	2155 ± 3	2160 ± 3	794 ± 9	782 ± 11
32	328 ± 0.28	706 ± 58	39 ± 3	0.0007041 ± 0.0000580	2199 ± 3	2205 ± 3	938 ± 17	919 ± 20
41	360 ± 0.39	502 ± 47	72 ± 7	0.0004561 ± 0.0000425	2264 ± 3	2271 ± 3	1102 ± 13	1090 ± 14
49	408 ± 0.31	544 ± 44	94 ± 8	0.0004366 ± 0.0000357	2240 ± 3	2248 ± 3	1389 ± 11	1377 ± 13
60	408 ± 0.23	930 ± 28	66 ± 2	0.0007456 ± 0.0000226	2244 ± 3	2255 ± 3	1660 ± 13	1639 ± 16
75	392 ± 0.26	448 ± 47	151 ± 16	0.0003747 ± 0.0000394	2260 ± 3	2272 ± 3	1902 ± 14	1891 ± 15
84	420 ± 0.42	364 ± 46	219 ± 28	0.0002840 ± 0.0000359	2250 ± 3	2263 ± 3	2103 ± 15	2095 ± 16

Table 2. LC-1 U-series data. Corrected ages use an average crustal value for the initial ^{230}Th/^{232}Th atomic ratio = 4.4 ± 2.2 ppm. Years before present = yrs BP, where present is 2010 CE. All errors are absolute 2σ. δ^{234}U = ([^{234}U/^{238}U]activity -1) x 1000. [^{230}Th/^{238}U] activity = 1 - $e^{-\lambda230T}$ + (δ^{234}U$_{measured}$/1000)[λ_{230}/(λ_{230} - λ_{234})](1 - $e^{-(\lambda230 - \lambda234)T}$), where T is the age. Decay constants (λ) are 9.1577 ×10^{-6} year^{-1} for ^{230}Th, 2.8263 × 10^{-6} year^{-1} for ^{234}U, and 1.55125 × 10^{-10} year^{-1} for ^{238}U.

Figure 4.2. LC-1 age model. The tip was set to zero age as LC-1 was collected from under an active drip. The tip corresponds to 0.5 mm depth along the pencil scale to which all dates are correlated. Dating uncertainties are smaller than the symbol used to represent the dates. The date removed from the age model due to contamination is indicated as a cross.
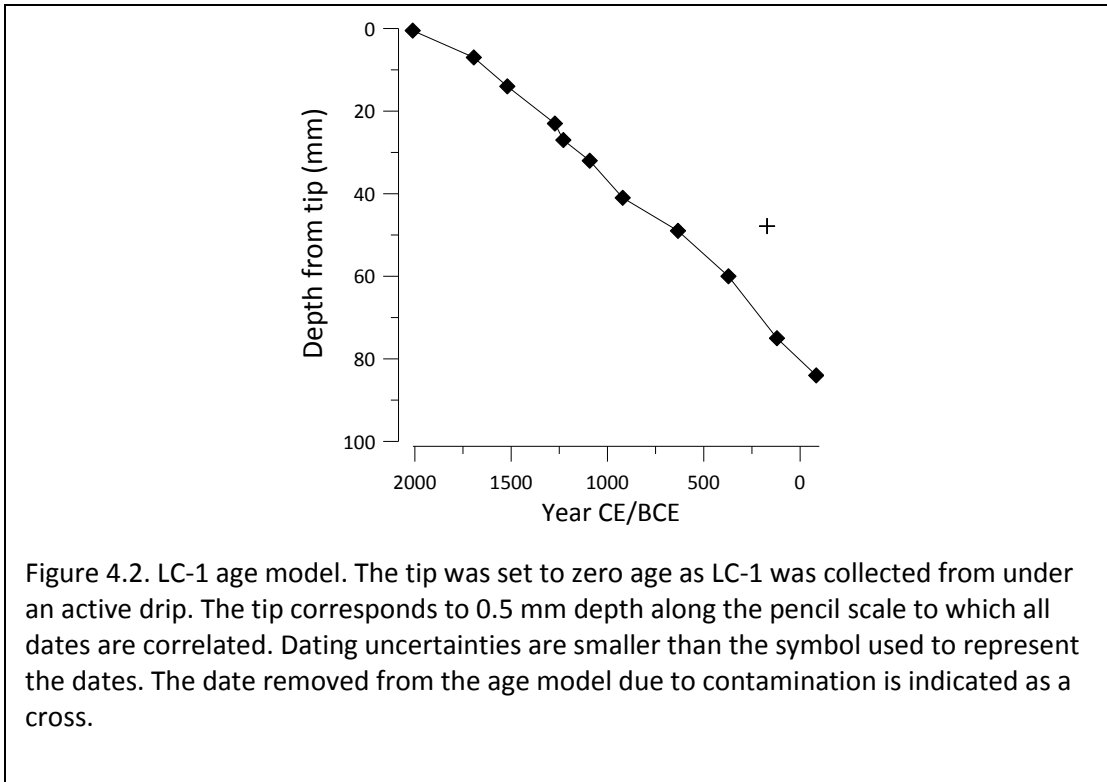
Oxygen Isotopes in Calcite

Analysis of the isotope ratios in LC-1 calcite resulted in 498 δ^{18}O values, ranging from -10.69 ‰ to -12.76 ‰ (Figure 4.3). Assuming that the measured cave temperature (8.27°C) is correct, the cave calcite precipitating from drip water that has a δ^{18}O value of -14.2 ‰ (the measured drip value for Leviathan cave) would theoretically have a δ^{18}O value of -11.5 ‰ (Feng et al., 2012). The range of δ^{18}O values in LC-1 and the δ^{18}O value of the most recent sample, -10.8 ‰, are in good agreement with the theoretical predicted values indicating that the calcite in LC-1 is precipitated at near-equilibrium conditions. Sampling resolution appears to be high enough to capture the true variations of cave drip water δ^{18}O values because the (lag 1) autocorrelation r^2 value is 0.78 throughout the time series. There is a linear trend with a slope of ~0.0002‰ per year and an intercept of -11.41‰ resulting in an ~0.4 ‰ increase in average for the length of

the record. The overall mean is ~11.64‰. The linear trend was removed from the raw $\delta^{18}O$

values and normalizing by the standard deviation (Figure 4.3).
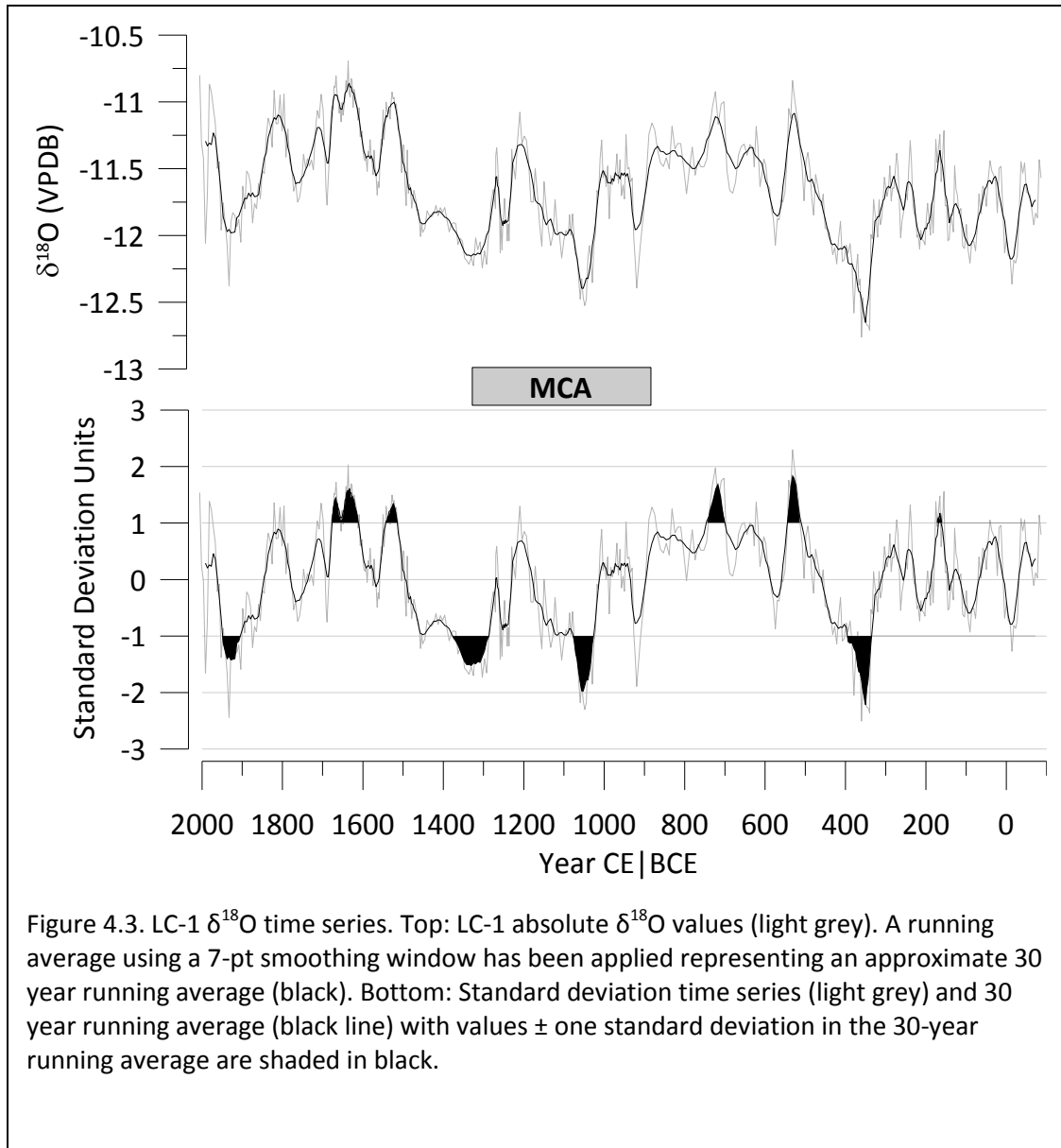
Figure 4.3. LC-1 $\delta^{18}O$ time series. Top: LC-1 absolute $\delta^{18}O$ values (light grey). A running average using a 7-pt smoothing window has been applied representing an approximate 30 year running average (black). Bottom: Standard deviation time series (light grey) and 30 year running average (black line) with values ± one standard deviation in the 30-year running average are shaded in black.

Deviations below (above) the mean value are interpreted to represent periods in which

there was an increase (decrease) in the relative percentage of winter time storms originating

from the northern Pacific. Periods in which $\delta^{18}O$ values are approximately more than one

standard deviation unit above or below the mean are assumed to represent periods of

"anomalous climate" variation at Leviathan Cave.

δ^{18}O values fluctuated between ~-11.1‰ and -12.2‰ around an average of -11.6‰,

during the interval of 100 BCE to 330 CE, but never exceeded greater variation than one

standard deviation unit. After this time, values dropped to -12.6‰ at 360 CE, 2 standard

deviation units below the mean, before steadily increasing to -10.7‰, 2 standard deviation units

above the mean, at 530 CE. During the interval of 330-530 CE, there was an ~ 100 year period

between 330 CE and 430 CE where values were consistently one standard deviation or greater

below the mean. This period is recognized as the oldest, centennial-scale, deviation from the

mean values in the record. Variation greater than one standard deviation, during this period,

only occurred on the decadal-scale between ~340 and 400 CE.

Between 500-1020 CE there were no centennial-scale periods in which values exceed

one standard deviation, above or below the mean, but values were generally greater than the

mean with the average δ^{18}O value for this time period being -11.5‰. During this ~620 year

period were several decadal-scale intervals, ~510-540 CE and ~695-740 CE, where δ^{18}O values

were continually more than one standard deviation unit greater than the mean. There is one

period, ~910-926 CE, when values were more than one standard deviation unit below the mean.

After 1020 CE, δ^{18}O values rapidly dropped to -12.5 ‰. During the interval of ~1040-

1140 CE values were approximately one standard deviation, or greater, below the mean δ^{18}O

value of -11.7‰ and this is interpreted as the second oldest centennial-scale climate anomaly in

the LC-1 reconstruction. During the interval 1140-1280 CE, δ^{18}O values averaged -11.7 ‰, very

close to the mean of the entire record, and never exceed more than one standard deviation unit

from the mean for more than a few years. After ~1280 CE, values were consistently at, or below,

one standard deviation from the mean until ~1490 CE. This two hundred year interval

represents the longest period in the LC-1 reconstruction in which values are one standard deviation or more from the mean.

Following this ~200 year period in which $\delta^{18}O$ values were consistently below the mean of the record, $\delta^{18}O$ values tended to be higher than the mean during 1500-1750 CE. During this interval the average $\delta^{18}O$ value is -11.4 ‰. There are two notable, decadal-scale periods contained in this larger 250 year period in which values were consistently greater than one standard deviation unit from the mean, 1515-1550 CE and ~1620-1715 CE. After 1750 CE, $\delta^{18}O$ values fluctuated within approximately one standard deviation unit of the mean until ~1850 CE when values began to decrease to the value of -12.6 ‰ at 1960 CE. Values were more than one standard deviation unit below the mean during the interval ~1890-1950 CE before fluctuating around the mean $\delta^{18}O$ value of the reconstruction until present.

The periods with the greatest departure from the mean $\delta^{18}O$ value (~2 standard deviation units) only occured on time scales less than 100 years. This implies the most extreme climatic anomalies in winter moisture source have been relatively short lived in the central Great Basin during the past 2000 years. Yet, there are much longer periods of anomalous climate, although inferred to be less extreme than the short lived events mentioned above, represented in the LC-1 reconstruction by approximately one standard deviation unit departure of the $\delta^{18}O$ value from the mean.

There are three centennial-scale periods (330-430 CE, 1040-1140 CE, and 1280-1490 CE), of decreased $\delta^{18}O$ values represented in the LC-1 reconstruction. Two of the centennial-scale events apparent in the LC-1 reconstruction, 1040-1140 CE and 1280-1490 CE, illustrate that anomalous climate associated with the recognized MCA time period (~850-1300 CE) occurred in the central Great Basin as two separate events. Although there was a small decrease

in $\delta^{18}O$ values around 910 CE, values quickly returned to near average levels by 1040-1140 CE. This suggests that more northern storm tracks were not persistent in the central Great Basin until 1040 CE. Anomalous $\delta^{18}O$ values around the MCA period were also not persistent. For example, from ~1140-1280 CE, $\delta^{18}O$ values returned to levels within one standard deviation of the mean and briefly exceeded (~1210 CE) more than one standard deviation unit above the mean, before they again dropped during 1280-1490 CE. From this it is interpreted that the MCA interval in the southern Great Basin should be considered as two separate intervals (1040-1140 CE and 1280-1490 CE), as these are the time intervals in which $\delta^{18}O$ stay near one standard deviation below the mean..

Spectral Analysis

Spectral analysis showed that significant variance at the 99% level occurs at the 9 and 16 year intervals. At the 95% level, significant variance occurs at 10, 14, and 18 year intervals. At the 90% level significant variance occurs at 20 years as well (Figure 4.4). It is noted that the 20 and 18 year intervals may be harmonics of the 10 and 9 year intervals, although this was not tested. Sampling resolution prevented resolution of frequencies below the ~8 year interval. This prevents drawing conclusions on the 2 to 8 year ENSO periodicity in LC-1.

Figure 4.4. δ^{18}O spectral analysis. Top: 99, 95, 90 and 80% (respective from the top down) confidence intervals. Years corresponding to frequency peaks greater than 95% confidence interval labeled.
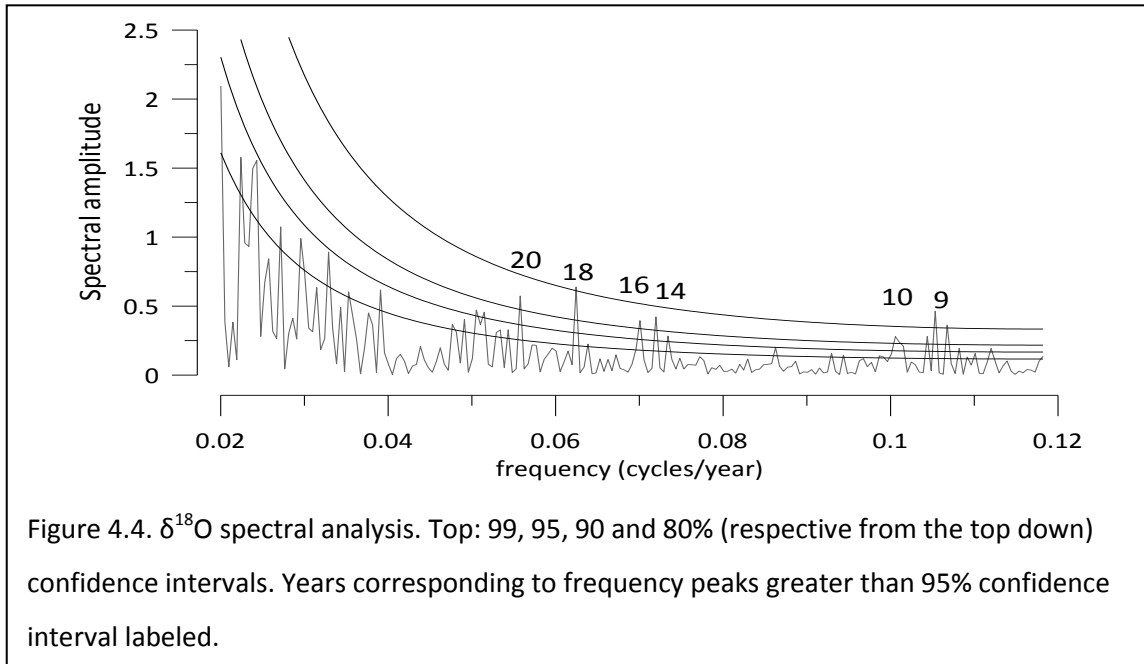
Results do indicate PDO scale variance is present in the LC-1 record as PDO is most energetic on the 15-20 year interval (Mantua and Hare, 2002). The PNA is active on time scales from weeks to decades, and has been shown to have a strong periodicity of 30 years (switching between phases every 15 years) during the past 300 years (Trouet and Taylor, 2009). Time series analysis suggests that the PNA periodicity reported by Trouet and Taylor (2009) may be present in LC-1 δ^{18}O time series as the 25-50 year periodicity is significant at the 80% confidence level (Table 3).

Significance Level	Frequency (Cycles Per Year)	Periodicity (Years per cycle)
99%	0.105; 0.062	9; 16
95%	0.099; 0.070; 0.055	10; 14; 18
90%	0.050;	20
80%	0.086; ~0.039-0.020; 0.014	12; ~25-50; 71

Table 3. δ^{18}O spectral analysis results. Table showing all significant frequencies and periodicity cycles for the same confidence intervals including those not pictured in Figure 4.4.

Wavelet Analysis

Wavelet analysis suggests statistically significant variance above the 95% confidence level for much of the record at the 10-30 year time scale. Peaks in variance for the 10-30 year band are centered at the dates ~10, ~410, ~540, ~1010, ~1510, and ~1960 years CE (Figure 4.5). Greatest variation occurring in the 10-30 year band supports the interpretation that there is a PNA and PDO signal in LC-1. Comparison of the wavelet analysis with the spectral analysis reveals that most of the variance in the 10-30 year band occurs in the 10-20 year range. The longest period of increased northern moisture source (~1100-1300 CE) corresponds with a period in which the 10-30 year periodicity has the weakest amplitude, suggesting that the driving climate modes operating on 10-30 year cycles may have become less prevalent during this interval.
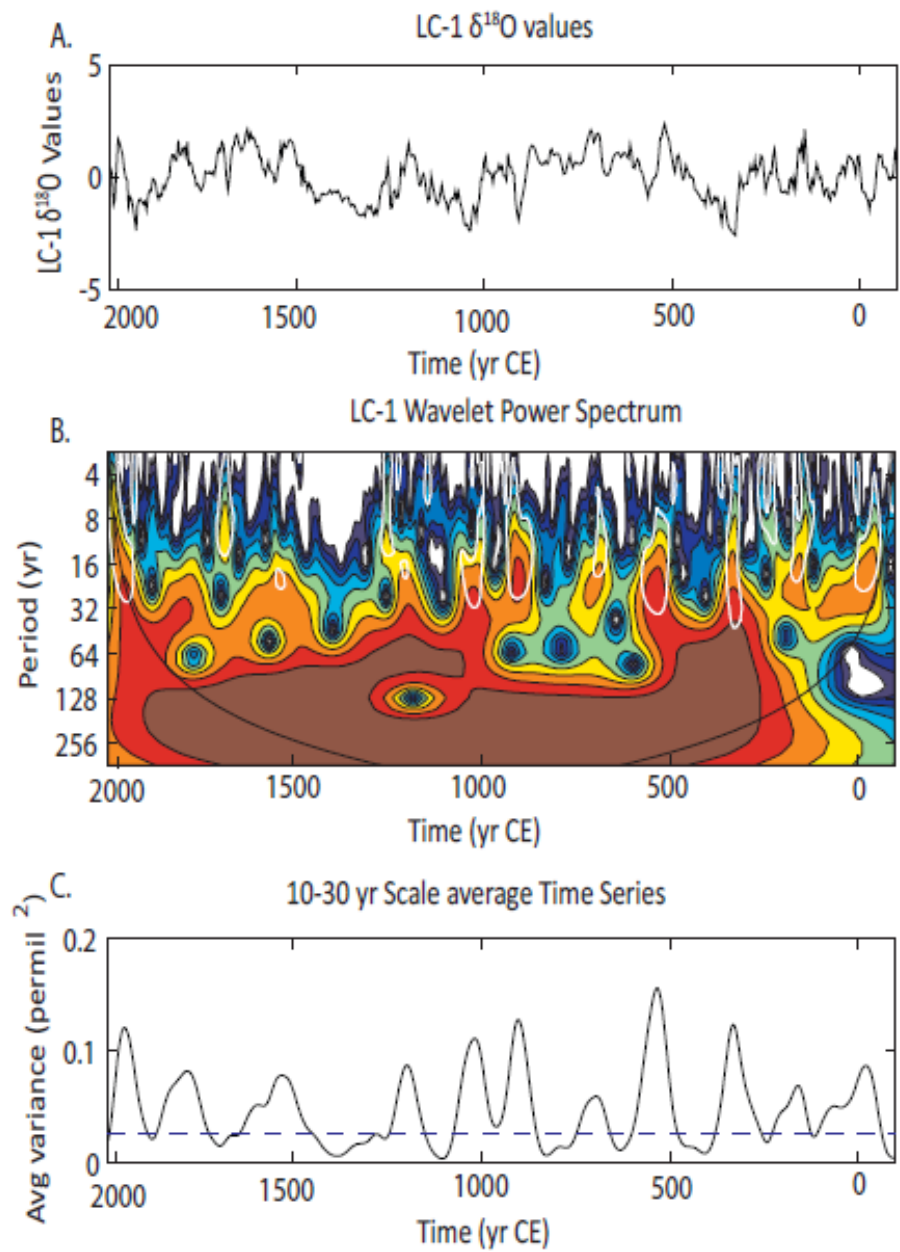
Figure 4.5. δ^{18}O wavelet analysis. A) LC-1 δ^{18}O detrended and normalized time series in standard deviation units. B) Wavelet spectrum for 4 year interpolated values with 95% confidence interval shown in white contours. The solid black line is the cone of influence, below which variations are not significant. C) 10-30 yr scale average time series. 95% confidence interval represented by dashed line.

Interpretation of δ^{18}O values

The δ^{18}O value of winter precipitation is strongly influenced by the latitude of source moisture arriving in the Great Basin (Friedman et al., 2002; Berkelhammer et al., 2012). From this, it is interpreted the δ^{18}O values in LC-1 speleothem calcite to be a proxy for winter moisture source variation over the past 2000 years. Additionally, because the PNA has a strong influence on winter moisture source in the area and is clearly expressed in precipitation δ^{18}O values (Liu et al., 2001), it is interpreted that LC-1 δ^{18}O variations are an indicator for the strength and phase of PNA. It is noted that both ENSO and PDO may modulate the atmospheric circulation parameters of which PNA is an index, so the ENSO and PDO signals are enveloped within the PNA index for a proxy reconstruction from a single location (Trouet and Taylor, 2009; Liu et la., 2011). More positive (negative) δ^{18}O values in LC-1 are interpreted to be indicative of a PPNA (RPNA) configuration. Based on this interpretation, it is suggested that the MCA in the Great Basin should be considered two separate intervals, ~1040-1140 CE and ~1280-1490 CE, which were characterized by a RPNA-state represented by anomalously low δ^{18}O in LC-1. Time series analysis of the LC-1 δ^{18}O suggests that the PNA system has operated primarily on a 10-20 year periodicity, in contrast to the 30 year periodicity reported by Trouet and Taylor (2009). It is possible that the difference in periodicity observed in the two records results from the PNA periodicity preserved in the LC-1 record was modulated by PDO and/or ENSO.

CHAPTER 5

DISCUSSION

Comparison to Other Pacific and North American Climate Mode Proxies

The variations in the δ^{18}O values of LC-1 are interpreted to be the result of changing

moisture source delivering precipitation to Leviathan Cave which is largely the result of the PNA

phase. That is, the PPNA (RPNA) phase is correlated to higher (lower) δ^{18}O values due to a more

southern-Pacific (northern-Pacific) moisture source. Yet, ENSO, PDO and PNA are all capable of

influencing atmospheric circulation patterns, as well as modulating the effects of each other, so

there is not a unique solution to any observed pattern in storm track variation. It has been

shown that ENSO and PDO modulate the occurrence frequency and strength of phase variations

in the PNA phenomena (Leathers et al., 1991; Yin, 1994; Trouet and Taylor; Liu et al., 2011). This

suggests that although LC-1 is a strong indicator of PNA phase, the PNA signal recorded in LC-1 is

modulated by ENSO and PDO, and therefore cannot be calibrated to create a strictly PNA index

independent of the inclusion of ENSO and PDO. Although, by using the relationships between

the extent of which ENSO, PDO and PNA may construct or diminish each other observed by

Trouet and Taylor (1999), and the examination of other proxy records, further attribution is

possible during a particular time interval. Discussion will focus on the MCA interval, although

similar logic may be applied to any time interval contained in the record.

To further investigate the hypothesis that LC-1 δ^{18}O values can be largely attributed to

PNA phase, I compared the δ^{18}O record to another proxy reconstruction of PNA. The most

extensive PNA reconstruction in the North American West was created by Trouet and Taylor

(2009), who reconstructed the PNA phase back to 1725 CE. The Trouet and Taylor (2009), record

was regressed against LC-1 using both a one-year interpolation of $\delta^{18}O$ values, and as an annually-interpolated 30-year running averages. The zero lag correlation r^2 values are 0.099 and 0.702, respectively (Figure 5.1). The high correlation for the smoothed data indicates that the two proxies share variance on the decadal to multi-decadal time scales but not the annual scale. This provides robust support for my interpretation that LC-1 $\delta^{18}O$ values are a strong indicator of PNA phase on the low-frequency decadal-scale. Thus, examination of LC-1 $\delta^{18}O$ values as an indicator of PNA phase during the MCA is appropriate. The LC-1 record indicates that a more

Figure 5.1. Correlation of the LC-1 $\delta^{18}O$ time series to a PNA index reconstruction. A) Annually interpolated LC-1 $\delta^{18}O$ values (light grey) and 30-year running average (black) from 1725-1999 CE. B) Annually resolved PNA index reconstruction (light grey) and 30-year running average (black) from 1725-1999 CE (Trouet and Taylor, 2009). C) Correlation between annual resolution LC-1 $\delta^{18}O$ values and PNA Index values. D) Correlation between 30-year running average LC-1 $\delta^{18}O$ values and PNA index values.

RPNA-like phase was present, from 1040-1140 CE and 1280-1490 CE, as these are centennial-scale intervals of more negative $\delta^{18}O$ values. Between these intervals, the PNA system appears to have been in a more mean or PPNA-like state indicated by an increase in $\delta^{18}O$ values. Further examination of ENSO and PDO is necessary to draw some conclusions on the extent in which these climate modes modulated the PNA signal represented in the LC-1 record. For comparison with the LC-1 data set, records containing at least the MCA period are included in this discussion. Several of these provide conflicting results preventing a definitive conclusion on the ENSO state during the MCA. A compilation of precipitation-sensitive records from regions affected by ENSO variations indicates that during the MCA El Niño occurrence was more common (Yan et al., 2011). Moy et al. (2002) presented a similar conclusion that El Niño frequency increased during the MCA (Figure 5.2). In contrast, work by Conroy et al. (2008) and Cobb et al. (2003) suggests that the ENSO system was in a La Niña state for at least part of the MCA. A reconstruction of PDO created by MacDonald and Case (2005), spanning the MCA period, extends back to 993 CE. Starting at 993 CE, the PDO was in a negative state, from which it steadily increased to a positive state at ~1500 CE. The LC-1 record indicates that the strongest expressions of a RPNA-like state observed in the record occurred from 1040-1140 CE and 1280-1490 CE. Trouet and Taylor (2009) observed that PNA can be amplified or diminished by ENSO and PDO and that the PNA can be positive under either positive or negative ENSO and PDO conditions, but no extremely negative PNA phases occur during extremely positive ENSO or PDO. As the MCA intervals represent the most extreme negative $\delta^{18}O$ excursions in the LC-1 record, the variation in moisture source is attributed to a RPNA phase, amplified by a negative PDO phase and the absence of a strong positive ENSO phase. It is possible that the ENSO system was in a more La Niña- like state or mild El Niño-like state. Although the presence of an extreme RPNA state suggests the absence of a strong El Niño state, it is noted that it is possible a strong

El Niño was present if the atmospheric teleconnections connecting the tropical Pacific to the

mid-latitudes were not stationary.

Figure 5.2 Comparison of Pacific Ocean climate mode proxies and LC-1 $\delta^{18}O$ values. A) $\delta^{18}O$ values of LC-1. B) PDO reconstruction (MacDonald and Case, 2006). C) Southern Oscillation Index (Yan et al., 2011). D) ENSO proxy based red intensity record of lake sediments from Laguna Pallcachoca (Moy et al., 2002). All bold lines represent approximately 30 year running averages.
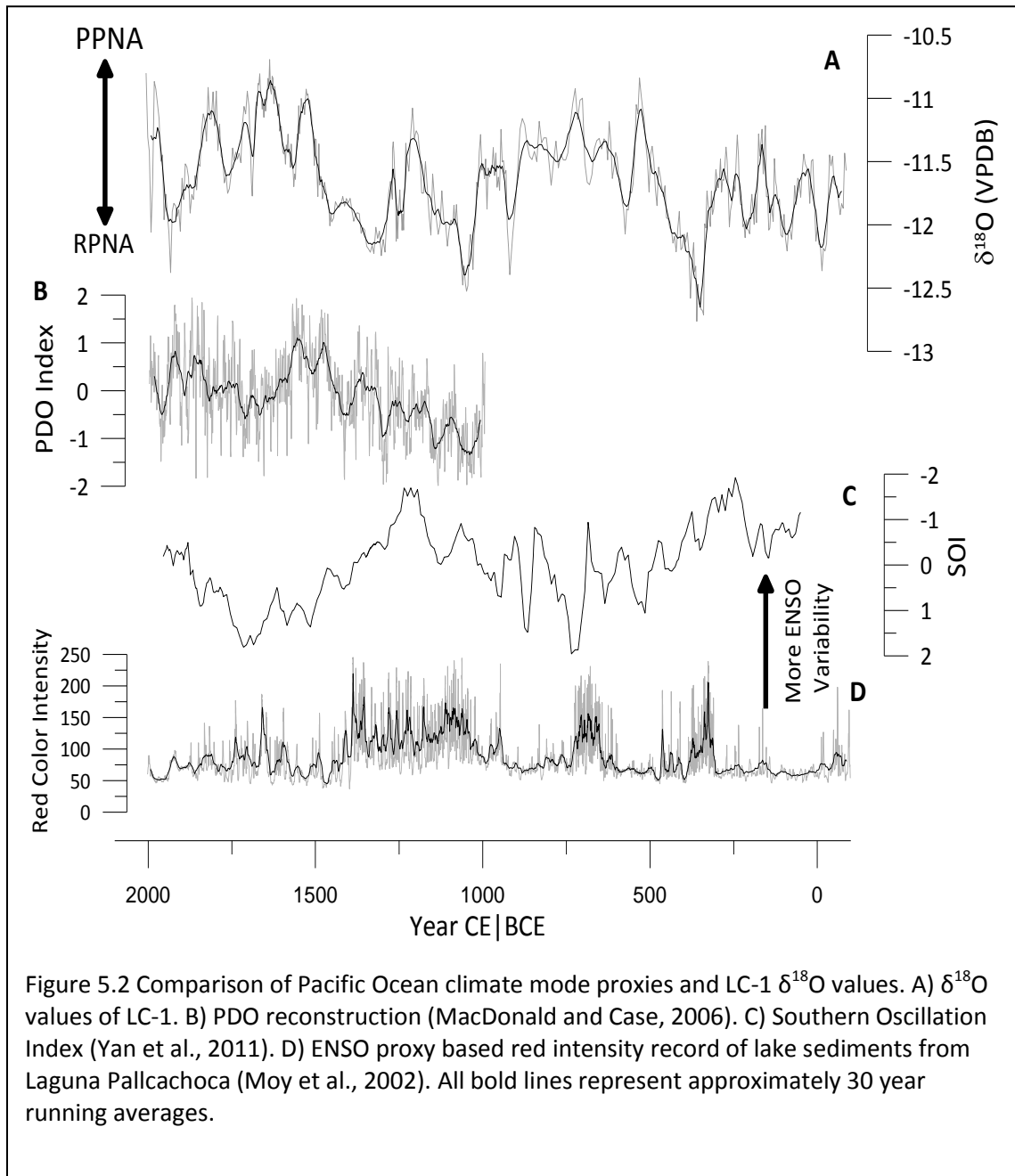
Regional Climatic Responses during the MCA

Comparison of climate characteristics represented in various proxy reconstructions at a particular time within a region presents its own challenges. Each climate proxy responds to a unique set of variables which may not be expressed in another proxy reconstruction. In addition, changes of a climate characteristic coordinated in time which changes in a different aspect of the climate system does not imply causation or a shared attribution. Under modern conditions there is not a strong correlation between precipitation amount during and PNA phase in the region of during the winter months (Leathers et al., 1991, Yin, 1994). While this prevents concluding a PNA causation for observed megadroughts of the past, comparison of paleoclimate proxies reveals temporal correlation between the changes in moisture source recorded in LC-1 and observed regional droughts during the MCA (Figure 5.3).
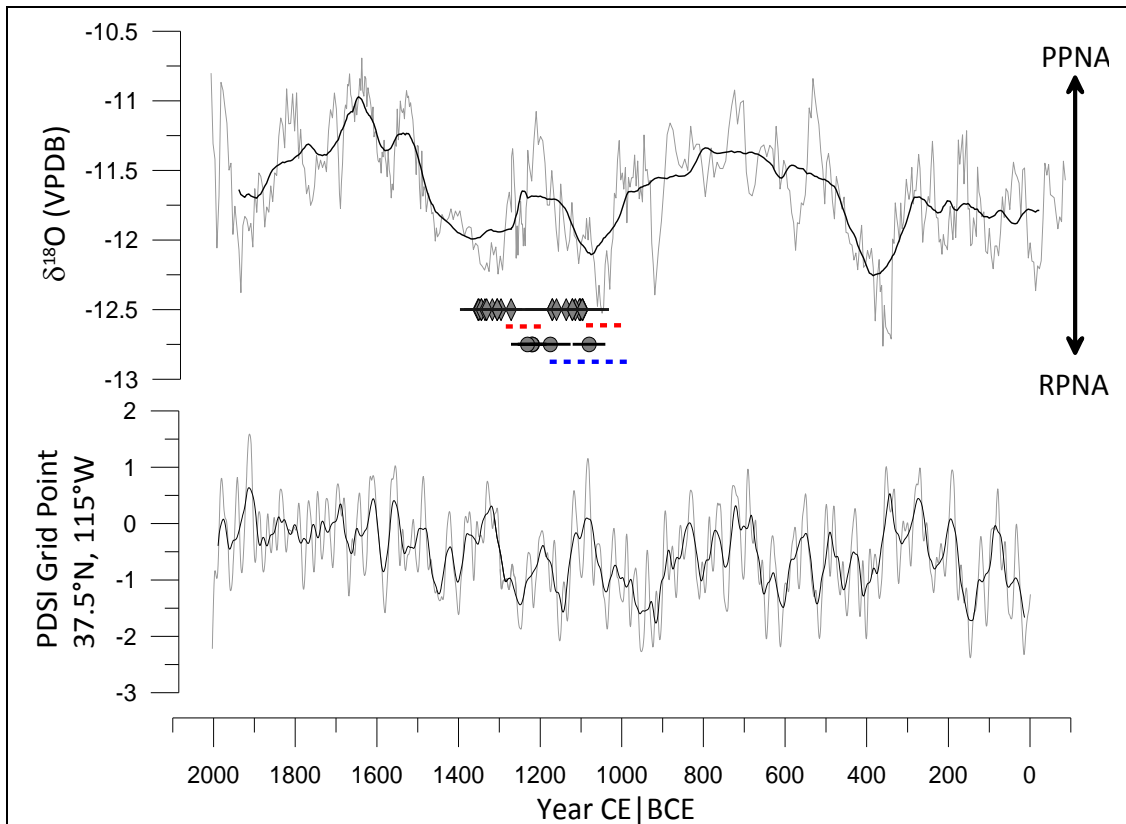
Figure 5.3. Comparison of Western U.S. and Great Basin paleoclimate proxies and LC-1 $\delta^{18}O$ values. Top: LC-1 $\delta^{18}O$ time series (light grey) with 30 year running average (black), interpretation of the direction of PPNA and RPNA indicated with arrow. Closed diamonds represent ^{14}C ages calibrated to calendar years of submerged littoral vegetation at Mono Lake, CA, (Stine, 1994) with dating uncertainties plotted as black bars. Red dashed line indicates approximate growth period for vegetation obtained through ring counting of dead trees. Closed circles represent death dates with dating uncertainties plotted as black bars of submerged vegetation at Fallen Leaf Lake, CA, (Kleppe et al, 2011). Blue dashed line indicates approximate growth period for vegetation at Fallen Leaf Lake. Bottom: PDSI reconstruction from grid point 37.5°N, 115°W (Cook et al., 2004).

To investigate the relationship between LC-1 $\delta^{18}O$ values and aridity, I compared my data to aridity proxy reconstructions from the Sierra Nevada and Great Basin. Documented low stands within lakes that are largely dependent on precipitation amount within their watershed to maintain their volume (as opposed to lakes in which changes in their inflow or outflow geomorphology accounts for lake volume) provide strong evidence for drought conditions.

45

Drought conditions at Mono Lake, CA, occurring during the MCA period are well documented and extensively studied (Stine, 1990; Stine, 1994; Benson et al., 2002; Benson et al., 2003). The death dates of littoral vegetation established during Mono Lake low stands and killed as a result of rising lake levels mark the transition from drought to pluvial conditions (Stine, 1994). Littoral vegetation appears to have grown for at least 100 years prior to being submerged based on the age of trees at time of death (Stine, 1994). Recalibration of the ^{14}C ages reported in the work by Stine (1994), to calendar years was necessary for comparison with the LC-1 reconstruction. To do this, the ^{14}C ages reported by Stine (1994), where recalibrated in OxCal 4.1 (Bronk Ramsey, 2009) using the IntCal09 calibration curve (Reimer et al., 2009) and are presented in Table 4.

Data reported in Stine, 1994.			Recalibrated Data					
	Radiocarbon Age		Cal BP (yrs)				Standard Form	
Sample ID	and uncertainty		From	To	%	sigma σ (±)	Median	uncertainty
1	930	±40	1040.5	1155	68.20	47	1102	47
2	910	±60	393.5	1793.5	68.20	675	932	675
3	860	±60	1052.5	1253	68.20	66	1170	66
4	890	±60	1045.5	1214.5	68.20	64	1136	64
5	940	±60	1030.5	1155.5	68.20	60	1102	60
6	920	±35	1043.5	1158.5	68.20	47	1104	47
7	950	±50	1025.5	1154.5	68.2	53	1096	53
8	920	±90	1028	1206	68.20	83	1114	83
9	860	±60	1052.5	1253	68.20	66	1170	66
10	940	±20	1036	1152	68.20	37	1096	37
11	870	±60	1046.5	1225	68.20	66	1160	66
12	700	±60	1259	1388.5	68.20	52	1296	52
13	600	±70	1300	1406.5	68.20	44	1352	44
14	640	±60	1286	1393.5	68.20	41	1344	41
15	730	±80	1215	1387	68.20	73	1271	73
16	675	±50	1275.5	1388.5	68.20	43	1317	43
17	570	±30	1320.5	1411.5	68.20	36	1350	36
18	690	±60	1264.5	1389	68.20	50	1305	50
19	950	±30	1029	1152	68.20	41	1097	41
20	904	±40	1044.5	1179	68.20	53	1121	53
21	640	±60	1286	1393.5	68.20	41	1344	41
22	660	±50	1281	1389.5	68.20	41	1335	41
23	690	±60	1264.5	1389	68.20	50	1305	50
24	660	±70	1277	1393.5	68.20	49	1331	49
25	910	±85	1035.5	1206	68.20	78	1121	78

Table 4. Recalibration table for ^{14}C radiocarbon dates reported in Stine (1994). Data was recalibrated in OxCal 4.1 (Bronk Ramsey, 2009) using the Intcal09 calibration curve (Reimer et al., 2009). Sample ID numbers correspond to the sample ID numbers presented in Stine (1994). Uncertainties are reported at the 68% level.

Death dates interpreted to represent drought terminations at Mono Lake occur in two

clusters centered at ~ 1130 CE and ~1300 CE. The earliest drought termination (~1130 CE) occurs

shortly after an inflection point in the LC-1 record indicating a transition from a more northern-

Pacific to more southern-Pacific moisture source interpreted to be a change from a RPNA-like

phase to PPNA phase. The second drought termination (~1300) coincides (within dating error of

vegetation) with an inflection point in the LC-1 record with the same relationship (RPNA to

PPNA) that occurred near the first drought termination. This suggests that during the MCA

conditions favoring the formation of an RPNA (PPNA) phase also favored the formation of

drought (pluvial) conditions. Similar to Mono Lake, submerged tree stumps at Fallen leaf Lake,

CA, (within the Lake Tahoe watershed) display death dates of ~1200 CE and growth ages of ~200

years prior to death. These data indicates lake regression must of occurred prior to ~1000 CE to

allow for growth to begin and lake transgression (to a level vegetation could no longer survive

along the shoreline) most have occurred at ~1200 CE (Kleppe et al., 2011).

The establishment of vegetation along the shoreline of the lake coincides with the end

of a several hundred year trend in decreasing LC-1 δ^{18}O values, interpreted to represent a

transition to a RPNA phase which ended at ~1050 CE. This suggests that as the PNA system

moved to an RPNA phase, lake levels dropped for a period of time sufficient for trees to become

established. This occurred at ~1200 CE, a time corresponding to the peak of a transition to a

more PPNA phase in the LC-1 record. This suggests conditions causing transition to a PPNA

phase also favor increased lake levels at Fallen Leaf Lake.

Dendroclimatic reconstructions provide another window into past climate conditions.

Cook et al. (2004) developed a grid of Palmer Drought Severity Index (PDSI) values based on

tree-ring reconstructions that span North America. The reconstruction from the nearest grid

47

point to Leviathan Cave (37.5°N, 115°W) is shown in Figure 5.3. The PDSI index quantifies

drought conditions using, precipitation, temperature, and soil properties during summer months

(Heim, 2002), and estimates of past PDSI were estimated from tree-ring reconstructions. There

are several problems with the index that should be kept in mind. It considers all precipitation as

rain, so it doesn't work well in higher elevations where a majority of precipitation occurs as

snow (National Oceanic and Atmospheric Administration, 2010). In addition, low-frequency

climate variation is difficult to determine and detect due to tree-ring standardization techniques

(Briffa et al., 2001).

Periods of negative PDSI are reported by Cook et al. (2007), to have occurred at ~890-

1080 CE, ~1100-1320 CE, and ~1380-1480 CE. During the time interval ~890-1480 CE there is a

generally negative PDSI value interrupted by two short intervals of approximately 30 years

centered at ~1100 CE and ~1310 CE in which the PDSI score rises to the approximate mean of

the record. These two peaks in PDSI values during the MCA chronologically correspond to lows

in $\delta^{18}O$ values in the LC-1 record. Lows in the $\delta^{18}O$ values of the LC-1 record are interpreted to

represent a more RPNA-like phase. This suggests that there may be a relationship between

summer PDSI increase, or wetter summers, and the RPNA phase.

Proxy-to-proxy comparison reveals that the observed droughts at Mono Lake and Fallen

Lake began at the approximate same time as shifts from PPNA to RPNA phases represented in

LC-1. Terminations of these droughts occur at points when the PNA phase shifts from RPNA back

to PPNA. This suggests that although PNA phase is not strongly correlated to precipitation

amounts from the instrumental records in the region of Leviathan Cave, on longer time scales

there is an association between the occurrence of RPNA-like storm tracks during the winter

months and decreased precipitation, such as during the MCA.

CHAPTER 6

CONCLUSIONS

Pacific Ocean circulations and related atmospheric circulations have a strong influence on climate across western North America through atmospheric teleconnections. Teleconnections are associations and statistically verifiable correlations among climate characteristics separated by distance. The three important modes of variability and teleconnections for the North American west are PNA, ENSO, and PDO, as they have been shown to have a strong influence on temperature and precipitation distribution through modulation of atmospheric circulation.

Of the past 2000 years, much attention has been given to the MCA period (~900-1350 CE) due to anomalous climate behavior observed in paleoclimate reconstructions and historical records (Lamb, 1965; Hughes and Diaz, 1994; Stine, 1994; Bradley et al., 2003). In the Great Basin and Sierra Nevada region the MCA has been determined to be an interval of severe and persistent drought occurrence (Stine, 1990; Stine, 1994; Benson et al., 2002; Cook et al., 2004; Kleppe et al., 2011). Drought in the region has been attributed to the alteration of precipitation distribution due to the Pacific Ocean being in a more negative ENSO state, negative PDO state and/or negative PNA (RPNA) state (Cook et al., 2007). PNA, ENSO, and PDO all have similar effects on atmospheric circulation and as well as the ability to modulate the effects of each other (Trouet and Taylor, 2010).

The δ^{18}O values of LC-1 are interpreted to be the result of storm track variation during the past 2000 years. Storm track variation and the δ^{18}O value of precipitation have been shown to be strongly correlated to the PNA phase (Leathers et al., 1991; Liu et al., 2011). Thus, LC-1 is

interpreted to be a strong indicator of PNA history. Around the MCA period (~1000-1500 CE) $\delta^{18}O$ values are generally below the mean $\delta^{18}O$ value for the record indicating the presence of a more RPNA-like atmospheric circulation configuration. Although, anomalous climate is most severe and sustained during the intervals ~1040-1140 CE and ~1280-1490 CE when $\delta^{18}O$ values drop to below or near one standard deviation of the mean. Between these two intervals values briefly return to near mean levels from 1140 to 1280 CE.

The co-occurrence of the reorganization of storm tracks to favor a greater contribution of precipitation originating from the North Pacific (represented in the LC-1 $\delta^{18}O$ values) and severe, persistent drought in the region during the MCA supports the hypothesis that these droughts occurred as a result of the presence of a RPNA, La Niña-like and/or negative PDO state. Droughts during the MCA appear to be the result of the decreased moisture originating from low latitudes. This is speculated to have occurred due to similar mechanisms as those observed during dry La Niña winters under modern conditions. This has important implications as it demonstrates the possibility for climate to shift to, and maintain, a state of persistent drought in the region due to changes in the temperature and energy flux within the atmosphere and oceans represented by ENSO, PDO and PNA. Further work is necessary to determine conclusively if these climate modes and teleconnection systems were stationary in the past and if they will continue to operate in the same manner into the future.

The single stalagmite record presented here is a large step forward in resolving past climate dynamics during the MCA. However, additional reconstructions should be pursued, both regionally and globally, from this time interval. Any single location or single proxy may not capture the true climate signal and is prone to bias introduced by local climate anomalies generating noise within the record. A more robust interpretation could be reached if additional over lapping records were created. Additionally, there is a need for further investigation into

potential correlations between $\delta^{18}O$ values in precipitation and ENSO and PDO phase. It is

speculated that a similar correlation exists between the phase of these systems and

precipitation $\delta^{18}O$ values as there is between the PNA phase and precipitation $\delta^{18}O$ values. The

principles and processes are very similar but careful analysis needs to be done to confirm this

inference.

APPENDIX I

STABLE ISOTOPE DATA

Dist from tip (mm)	$\delta^{18}O$ (VPDB)	Year CE	Dist from tip (mm)	$\delta^{18}O$ (VPDB)	Year CE	Dist from tip (mm)	$\delta^{18}O$ (VPDB)	Year CE
0.1	-10.80	2006.12	5.2	-11.71	1757.40	10.3	-11.37	1599.54
0.2	-11.31	2001.25	5.3	-11.61	1752.52	10.4	-11.43	1597.06
0.3	-11.42	1996.37	5.4	-11.39	1747.65	10.5	-11.44	1594.57
0.4	-12.06	1991.49	5.5	-11.49	1742.77	10.6	-11.41	1592.09
0.5	-11.68	1986.62	5.6	-11.43	1737.89	10.7	-11.52	1589.60
0.6	-10.87	1981.74	5.7	-11.48	1733.02	10.8	-11.37	1587.12
0.7	-10.92	1976.86	5.8	-11.43	1728.14	10.9	-11.40	1584.63
0.8	-11.05	1971.99	5.9	-11.51	1723.26	11.0	-11.28	1582.14
0.9	-11.16	1967.11	6.0	-11.22	1718.39	11.1	-11.40	1579.66
1.0	-11.50	1962.23	6.1	-11.06	1713.51	11.2	-11.45	1577.17
1.1	-11.45	1957.35	6.2	-11.12	1708.63	11.3	-11.55	1574.69
1.2	-11.96	1952.48	6.3	-10.94	1703.76	11.4	-11.36	1572.20
1.3	-11.76	1947.60	6.4	-11.06	1698.88	11.5	-11.50	1569.72
1.4	-11.91	1942.72	6.5	-11.42	1694.00	11.6	-11.54	1567.23
1.5	-12.07	1937.85	6.6	-11.67	1691.52	11.7	-11.70	1564.74
1.6	-12.38	1932.97	6.7	-11.77	1689.03	11.8	-11.60	1562.26
1.7	-11.90	1928.09	6.8	-11.59	1686.54	11.9	-11.64	1559.77
1.8	-11.83	1923.22	6.9	-11.45	1684.06	12.0	-11.40	1557.29
1.9	-11.85	1918.34	7.0	-11.24	1681.57	12.1	-11.28	1554.80
2.0	-11.93	1913.46	7.1	-11.08	1679.09	12.2	-11.33	1552.32
2.1	-11.88	1908.59	7.2	-11.03	1676.60	12.3	-11.06	1549.83
2.2	-12.05	1903.71	7.3	-11.06	1674.12	12.4	-11.28	1547.34
2.3	-11.63	1898.83	7.4	-10.88	1671.63	12.5	-11.18	1544.86
2.4	-11.80	1893.95	7.5	-10.89	1669.14	12.6	-11.00	1542.37
2.5	-11.52	1889.08	7.6	-10.81	1666.66	12.7	-11.07	1539.89
2.6	-11.54	1884.20	7.7	-10.96	1664.17	12.8	-11.08	1537.40
2.7	-11.63	1879.32	7.8	-10.99	1661.69	12.9	-11.06	1534.92
2.8	-11.91	1874.45	7.9	-11.08	1659.20	13.0	-11.13	1532.43
2.9	-11.76	1869.57	8.0	-11.04	1656.72	13.1	-11.01	1529.94
3.0	-11.80	1864.69	8.1	-11.15	1654.23	13.2	-10.93	1527.46
3.1	-11.61	1859.82	8.2	-11.01	1651.74	13.3	-10.98	1524.97
3.2	-11.72	1854.94	8.3	-11.10	1649.26	13.4	-10.97	1522.49
3.3	-11.52	1850.06	8.4	-11.03	1646.77	13.5	-11.04	1520.00
3.4	-11.54	1845.19	8.5	-10.96	1644.29	13.6	-11.01	1517.26
3.5	-11.25	1840.31	8.6	-10.84	1641.80	13.7	-11.09	1514.52
3.6	-11.12	1835.43	8.7	-10.92	1639.32	13.8	-11.14	1511.77
3.7	-11.17	1830.56	8.8	-10.69	1636.83	13.9	-11.25	1509.03
3.8	-11.34	1825.68	8.9	-10.93	1634.34	14.0	-11.35	1506.28
3.9	-10.91	1820.80	9.0	-10.97	1631.86	14.1	-11.53	1503.54
4.0	-11.16	1815.92	9.1	-10.83	1629.37	14.2	-11.32	1500.80
4.1	-11.16	1811.05	9.2	-10.84	1626.89	14.3	-11.33	1498.05
4.2	-10.95	1806.17	9.3	-11.04	1624.40	14.4	-11.62	1495.31
4.3	-11.22	1801.29	9.4	-10.91	1621.92	14.5	-11.78	1492.56
4.4	-10.94	1796.42	9.5	-10.95	1619.43	14.6	-11.36	1489.82
4.5	-11.41	1791.54	9.6	-10.98	1616.94	14.7	-11.68	1487.07
4.6	-11.20	1786.66	9.7	-11.04	1614.46	14.8	-11.62	1484.33
4.7	-11.45	1781.79	9.8	-11.14	1611.97	14.9	-11.65	1481.58
4.8	-11.49	1776.91	9.9	-11.04	1609.49	15.0	-11.80	1478.84
4.9	-11.67	1772.03	10.0	-11.26	1607.00	15.1	-11.73	1476.10
5.0	-11.61	1767.16	10.1	-11.23	1604.52	15.2	-11.66	1473.35
5.1	-11.75	1762.28	10.2	-11.22	1602.03	15.3	-11.70	1470.61

Note: $\delta^{18}O$ values represented in ‰ notation

Dist from tip (mm)	δ¹⁸O (VPDB)	Year CE	Dist from tip (mm)	δ¹⁸O (VPDB)	Year CE	Dist from tip (mm)	δ¹⁸O (VPDB)	Year CE
15.4	-11.74	1467.86	25.0	-11.89	1245.50	35.1	-11.99	1021.70
15.5	-11.81	1465.12	25.2	-11.89	1243.30	35.3	-11.66	1017.90
15.6	-11.80	1462.37	25.4	-12.04	1241.10	35.5	-11.70	1014.10
15.7	-11.88	1459.63	25.6	-11.91	1238.90	35.7	-11.42	1010.30
15.8	-12.01	1456.88	25.8	-12.04	1236.70	35.9	-11.29	1006.50
15.9	-11.91	1454.14	26.0	-11.77	1234.50	36.1	-11.57	1002.70
16.0	-11.98	1451.40	26.2	-11.71	1232.30	36.3	-11.52	998.90
16.2	-11.95	1445.91	26.4	-11.36	1230.10	36.5	-11.63	995.10
16.4	-11.82	1440.42	26.6	-11.44	1227.90	36.7	-11.48	991.30
16.6	-11.85	1434.93	26.8	-11.58	1220.78	36.9	-11.88	987.50
16.8	-11.86	1429.44	27.0	-11.28	1215.30	37.1	-11.55	983.70
17.0	-11.84	1423.95	27.2	-11.08	1209.82	37.3	-11.62	979.90
17.2	-11.78	1418.46	27.4	-11.31	1204.34	37.5	-11.55	976.10
17.4	-11.85	1412.97	27.6	-11.26	1198.86	37.7	-11.55	972.30
17.6	-11.79	1407.49	27.8	-11.29	1193.38	37.9	-11.39	968.50
17.8	-11.83	1402.00	28.0	-11.45	1187.90	38.1	-11.61	964.70
18.0	-11.79	1396.51	28.2	-11.75	1182.42	38.3	-11.43	960.90
18.2	-11.89	1391.02	28.4	-11.75	1176.94	38.5	-11.70	957.10
18.4	-11.97	1385.53	28.6	-11.50	1171.46	38.7	-11.62	953.30
18.6	-11.92	1380.04	28.8	-11.70	1165.98	38.9	-11.73	949.50
18.8	-11.90	1374.55	29.0	-11.93	1160.50	39.1	-11.25	945.70
19.0	-11.91	1369.06	29.2	-12.08	1155.02	39.3	-11.50	941.90
19.2	-12.07	1363.58	29.4	-11.60	1149.54	39.5	-11.49	938.10
19.4	-12.02	1358.09	29.6	-11.81	1144.06	39.7	-11.60	934.30
19.6	-12.04	1352.60	29.8	-11.96	1138.58	39.9	-11.57	930.50
19.8	-12.17	1347.11	30.0	-12.08	1133.10	40.1	-12.02	926.70
20.0	-12.19	1341.62	30.1	-12.00	1127.62	40.3	-12.18	922.90
20.2	-12.22	1336.13	30.3	-11.73	1122.14	40.5	-12.39	919.10
20.4	-12.16	1330.64	30.5	-11.97	1116.66	40.7	-12.07	910.24
20.6	-12.23	1325.15	30.7	-11.99	1111.18	40.9	-11.87	903.07
20.8	-12.02	1319.66	30.9	-12.17	1105.70	41.1	-11.57	895.89
21.0	-12.11	1314.18	31.1	-12.03	1100.22	41.3	-11.24	888.72
21.2	-12.05	1308.69	31.3	-11.96	1094.74	41.5	-11.16	881.54
21.4	-12.24	1303.20	31.5	-11.99	1089.26	41.7	-11.21	874.37
21.6	-12.12	1297.71	31.7	-11.85	1086.30	41.9	-11.36	867.19
21.8	-12.22	1292.22	31.9	-12.00	1082.50	42.1	-11.46	860.02
22.0	-11.95	1286.73	32.1	-11.84	1078.70	42.3	-11.48	852.84
22.2	-11.75	1281.24	32.3	-12.01	1074.90	42.5	-11.42	845.67
22.4	-11.66	1275.75	32.5	-12.09	1071.10	42.7	-11.50	838.49
22.6	-11.80	1270.27	32.7	-12.16	1067.30	42.9	-11.18	831.32
22.8	-11.40	1269.70	32.9	-12.33	1063.50	43.1	-11.35	824.14
23.0	-11.34	1267.50	33.1	-12.48	1059.70	43.3	-11.31	816.97
23.2	-11.43	1265.30	33.3	-12.33	1055.90	43.5	-11.31	809.79
23.4	-11.58	1263.10	33.5	-12.47	1052.10	43.7	-11.49	802.62
23.6	-11.70	1260.90	33.7	-12.53	1048.30	43.9	-11.69	795.44
23.8	-12.13	1258.70	33.9	-12.48	1044.50	44.1	-11.50	788.27
24.0	-11.90	1256.50	34.1	-12.17	1040.70	44.3	-11.34	781.09
24.2	-12.11	1254.30	34.3	-12.08	1036.90	44.5	-11.55	773.92
24.4	-11.91	1252.10	34.5	-12.19	1033.10	44.7	-11.44	766.74
24.6	-11.83	1249.90	34.7	-12.35	1029.30	44.9	-11.49	759.57
24.8	-11.72	1247.70	34.9	-12.07	1025.50	45.1	-11.49	752.39

Note: δ¹⁸O values represented in ‰ notation

Dist from tip (mm)	δ¹⁸O (VPDB)	Year CE	Dist from tip (mm)	δ¹⁸O (VPDB)	Year CE	Dist from tip (mm)	δ¹⁸O (VPDB)	Year CE
45.3	-11.43	745.22	55.5	-11.70	464.89	65.7	-11.74	266.16
45.5	-11.20	738.04	55.7	-11.78	460.13	65.9	-12.02	262.80
45.7	-11.04	730.87	55.9	-11.69	455.36	66.1	-11.89	259.44
45.9	-10.92	723.69	56.1	-11.95	450.60	66.3	-11.83	256.08
46.1	-11.17	716.52	56.3	-11.95	445.84	66.5	-11.76	252.72
46.3	-11.01	709.34	56.5	-12.02	441.07	66.7	-11.69	249.36
46.5	-11.00	702.17	56.7	-12.04	436.31	66.9	-11.73	246.00
46.7	-11.51	694.99	56.9	-12.14	431.54	67.1	-11.49	242.64
46.9	-11.66	687.82	57.1	-12.09	426.78	67.3	-11.29	239.28
47.1	-11.68	680.64	57.3	-12.21	422.02	67.5	-11.45	235.92
47.3	-11.60	673.47	57.5	-12.03	417.25	67.7	-11.77	232.56
47.5	-11.40	666.29	57.7	-11.89	412.49	67.9	-11.84	229.20
47.7	-11.33	659.12	57.9	-12.20	407.73	68.1	-11.84	225.84
47.9	-11.32	651.94	58.1	-12.18	402.96	68.3	-12.01	222.48
48.1	-11.40	644.77	58.3	-12.07	398.20	68.5	-11.99	219.12
48.3	-11.32	637.59	58.5	-12.13	393.44	68.7	-12.10	215.76
48.5	-11.35	630.42	58.7	-12.06	388.67	68.9	-11.96	212.40
48.7	-11.49	626.85	58.9	-12.20	383.91	69.1	-12.03	209.04
48.9	-11.18	622.09	59.1	-12.58	379.14	69.3	-12.04	205.68
49.1	-11.35	617.33	59.3	-12.28	374.38	69.5	-12.07	202.32
49.3	-11.63	612.56	59.5	-12.14	369.62	69.7	-11.86	198.96
49.5	-11.55	607.80	59.7	-12.37	366.96	69.9	-11.76	195.60
49.7	-11.43	603.04	59.9	-12.33	363.60	70.1	-11.89	192.24
49.9	-11.47	598.27	60.1	-12.76	360.24	70.3	-12.00	188.88
50.1	-11.63	593.51	60.3	-12.47	356.88	70.5	-11.76	185.52
50.3	-11.65	588.74	60.5	-12.62	353.52	70.7	-11.98	182.16
50.5	-11.80	583.98	60.7	-12.65	350.16	70.9	-11.70	178.80
50.7	-11.87	579.22	60.9	-12.67	346.80	71.1	-11.28	175.44
50.9	-12.07	574.45	61.1	-12.68	343.44	71.3	-11.46	172.08
51.1	-11.87	569.69	61.3	-12.71	340.08	71.5	-11.35	168.72
51.3	-11.88	564.93	61.5	-11.99	336.72	71.7	-11.24	165.36
51.5	-11.73	560.16	61.7	-12.02	333.36	71.9	-11.60	162.00
51.7	-11.75	555.40	61.9	-11.73	330.00	72.1	-11.41	158.64
51.9	-11.68	550.64	62.1	-11.83	326.64	72.3	-11.22	155.28
52.1	-11.45	545.87	62.3	-11.91	323.28	72.5	-11.78	151.92
52.3	-11.05	541.11	62.5	-12.01	319.92	72.7	-11.77	148.56
52.5	-11.12	536.34	62.7	-11.73	316.56	72.9	-12.04	145.20
52.7	-10.84	531.58	62.9	-11.92	313.20	73.1	-12.03	141.84
52.9	-10.97	526.82	63.1	-11.87	309.84	73.3	-11.84	138.48
53.1	-11.08	522.05	63.3	-11.73	306.48	73.5	-11.90	135.12
53.3	-11.17	517.29	63.5	-11.56	303.12	73.7	-11.97	131.76
53.5	-11.37	512.53	63.7	-11.65	299.76	73.9	-11.48	128.40
53.7	-11.50	507.76	63.9	-11.71	296.40	74.1	-11.65	125.04
53.9	-11.74	503.00	64.1	-11.65	293.04	74.3	-11.70	121.68
54.1	-11.44	498.24	64.3	-11.48	289.68	74.5	-11.83	118.32
54.3	-11.38	493.47	64.5	-11.74	286.32	74.7	-11.80	113.17
54.5	-11.50	488.71	64.7	-11.64	282.96	74.9	-12.08	108.64
54.7	-11.72	483.94	64.9	-11.65	279.60	75.1	-12.10	104.11
54.9	-11.85	479.18	65.1	-11.52	276.24	75.3	-11.92	99.57
55.1	-11.54	474.42	65.3	-11.39	272.88	75.5	-12.11	95.04
55.3	-11.61	469.65	65.5	-11.48	269.52	75.7	-12.21	90.51

Note: δ¹⁸O values represented in ‰ notation

Dist from tip (mm)	δ¹⁸O (VPDB)	Year CE
75.9	-12.04	85.97
76.1	-12.04	81.44
76.3	-12.11	76.91
76.5	-11.94	72.37
76.7	-11.69	67.84
76.9	-11.84	63.31
77.1	-11.63	58.77
77.3	-11.65	54.24
77.5	-11.78	49.71
77.7	-11.58	45.17
77.9	-11.44	40.64
78.1	-11.52	36.11
78.3	-11.55	31.57
78.5	-11.59	27.04
78.7	-11.83	22.51
78.9	-11.50	17.97
79.1	-11.48	13.44
79.3	-11.80	8.91
79.5	-12.13	4.37
79.7	-12.02	-0.16
79.9	-12.15	-4.69
80.1	-12.16	-9.23
80.3	-12.36	-13.76
80.5	-12.19	-18.29
80.7	-12.21	-22.83
80.9	-12.15	-27.36
81.1	-11.85	-31.89
81.3	-11.45	-36.43
81.5	-11.53	-40.96
81.7	-11.46	-45.49
81.9	-11.67	-50.03
82.1	-11.68	-54.56
82.3	-11.70	-59.09
82.5	-11.82	-63.63
82.7	-11.92	-68.16
82.9	-11.83	-72.69
83.1	-11.87	-77.23
83.4	-11.43	-81.76
83.6	-11.57	-86.29

Note: δ¹⁸O values represented in ‰ notation

REFERENCES

Barnett, T.P., and Pierce, D.W., 2008, When will Lake Mead go dry?: Water Resources Research, v. 44, no. 3, p. W03201.

Beaty, R.M., and Taylor, A.H., 2009, A 14 000 year sedimentary charcoal record of fire from the northern Sierra Nevada, Lake Tahoe Basin, California, USA: The Holocene, v. 19, no. 3, p. 347-358.

Benson, L., Kashgarian, M., Rye, R., et al., 2002, Holocene multidecadal and multicentennial droughts affecting Northern California and Nevada: Quaternary Science Reviews, v. 21, no. 4-6, p. 659-682.

Benson, L., Liddicoat, J., Smoot, J., Sarna-Wojcicki, A., Negrini, R., and Lund, S., 2003, Age of the Mono Lake excursion and associated tephra: Quaternary Science Reviews, v. 22, no. 2-4, p. 135-140.

Berkelhammer, M., Stott, L., Yoshimura, K., Johnson, K., and Sinha, A., 2012, Synoptic and mesoscale controls on the isotopic composition of precipitation in the western United States, Springer Berlin / Heidelberg 38, 433 p.

Biondi, F., Gershunov, A., and Cayan, D.R., 2001, North Pacific Decadal Climate Variability since 1661: Journal of Climate, v. 14, no. 1, p. 5-10.

Bradley, R.S., Hughes, M.K., and Diaz, H.F., 2003, Climate in Medieval Time: Science, v. 302, no. 5644, p. 404-405.

Briffa, K.R., Osborn, T.J., Schweingruber, F.H., Harris, I.C., Jones, P.D., Shiyatov, S.G., and Vaganov, E.A., 2001, Low-frequency temperature variations from a northern tree ring density network, v. 106, p. 2929-2941.

Cheng, H., Edwards, R.L., Hoff, J., Gallup, C.D., Richards, D.A., and Asmerom, Y., 2000, The half-lives of uranium-234 and thorium-230: Chemical Geology, v. 169, no. 1–2, p. 17-33.

Cobb, K.M., Charles, C.D., Cheng, H., and Edwards, R.L., 2003, El Nino/Southern Oscillation and tropical Pacific climate during the last millennium: Nature, v. 424, no. 6946, p. 271-276.

Cole, J.E., Overpeck, J.T., and Cook, E.R., 2002, Multiyear La Niï¿½a events and persistent drought in the contiguous United States: Geophysical Research Letters, v. 29, no. 13, p. 1647.

Conroy, J.L., Overpeck, J.T., Cole, J.E., Shanahan, T.M., and Steinitz-Kannan, M., 2008, Holocene changes in eastern tropical Pacific climate inferred from a Galápagos lake sediment record: Quaternary Science Reviews, v. 27, no. 11-12, p. 1166-1180.

Conroy, J.L., Overpeck, J.T., Cole, J.E., and Steinitz-Kannan, M., 2009, Variable oceanic influences on western North American drought over the last 1200 years: Geophysical Research Letters, v. 36, no. 17, p. L17703.

Cook, E.R., Palmer, J.G., and D'Arrigo, R.D., 2002, Evidence for a 'Medieval Warm Period' in a 1,100 year tree-ring reconstruction of past austral summer temperatures in New Zealand: Geophysical Research Letters, v. 29, no. 14, p. 1667.

Cook, E.R., Seager, R., Cane, M.A., and Stahle, D.W., 2007, North American drought: Reconstructions, causes, and consequences: Earth-Science Reviews, v. 81, no. 1-2, p. 93-134.

Cook, E.R., Woodhouse, C.A., Eakin, C.M., Meko, D.M., and Stahle, D.W., 2004, Long-Term Aridity Changes in the Western United States: Science, v. 306, no. 5698, p. 1015-1018.

Crafford, A.E.J., 2007, **Geologic Map of Nevada: U.S. Geological Survey Data Series 249 [map]**, v. 46 p, no. 1-plate.

Fairchild, I.J., Smith, C.L., Baker, A., et al., 2006, Modification and preservation of environmental signals in speleothems: Earth-Science Reviews, v. 75, no. 1-4, p. 105-153.

Feng, W., Banner, J., Guilfoyle, A., Musgrove, M., and James, E., 2012, Oxygen isotopic fractionation between drip waterand speleothem calcite: A 10-year monitoring study, central Texas, USA.: Chemical Geology, v. 304-305, p. 53-67.

Friedman, I., Harris, J.M., Smith, G.I., and Johnson, C.A., 2002, Stable isotope composition of waters in the Great Basin, United States 1. Air-mass trajectories, v. 107, p. 4400.

Graham, N.E., and Hughes, M.K., 2007, Reconstructing the Mediaeval low stands of Mono Lake, Sierra Nevada, California, USA: The Holocene, v. 17, no. 8, p. 1197-1210.

Graham, N., Hughes, M., Ammann, C., et al., 2007, Tropical Pacific – mid-latitude teleconnections in medieval times, Springer Netherlands 83, 241 p.

Heim, R.R., 2002, A Review of Twentieth-Century Drought Indices Used in the United States: Bulletin of the American Meteorological Society, v. 83, no. 8, p. 1149-1165.

Hendy, C.H., 1971, The isotopic geochemistry of speleothems—I. The calculation of the effects of different modes of formation on the isotopic composition of speleothems and their applicability as palaeoclimatic indicators: Geochimica et Cosmochimica Acta, v. 35, no. 8, p. 801-824.

Herweijer, C., Seager, R., and Cook, E.R., 2006, North American droughts of the mid to late nineteenth century: a history, simulation and implication for Mediaeval drought: The Holocene, v. 16, no. 2, p. 159-171.

Hughes, M.K., and Diaz, H.F., 1994, Was there a ˜medieval warm period', and if so, where and when?: Climatic Change, v. 26, no. 2, p. 109-142.

Hughes, M., and Funkhouser, G., 1998, Extremes of moisture availability reconstructed from tree rings for recent millennia in the great basin of western north America. *in* Beniston, M. and Innes, J., eds., The Impacts of Climate Variability on Forests, Springer Berlin / Heidelberg 74, p.99-107.

Jaffey, A.H., Flynn, K.F., Glendenin, L.E., Bentley, W.C., and Essling, A.M., 1971, Precision Measurement of Half-Lives and Specific Activities of [235]U and [238]U: Physical Review C, v. 4, no. 5, p. 1889-1906.

Jones, P.D., and Mann, M.E., 2004, Climate Over Past Millennia: Reviews of Geophysics, v. 42, p. RG2002.

Kim, S., and O'Neil, J.R., 1997, Equilibrium and nonequilibrium oxygen isotope effects in synthetic carbonates: Geochimica et Cosmochimica Acta, v. 61, no. 16, p. 3461-3475.

Kleppe, J.A., Brothers, D.S., Kent, G.M., Biondi, F., Jensen, S., and Driscoll, N.W., 2011, Duration and severity of Medieval drought in the Lake Tahoe Basin: Quaternary Science Reviews, no. 0.

Kurtzman, D., and Scanlon, B.R., 2007, El Niño–Southern Oscillation and Pacific Decadal Oscillation impacts on precipitation in the southern and central United States: Evaluation of spatial distribution and predictions: Water Resources Research, v. 43, no. 10, p. W10427.

Lachniet, M.S., 2009, Climatic and environmental controls on speleothem oxygen-isotope values: Quaternary Science Reviews, v. 28, no. 5-6, p. 412-432.

Lachniet, M.S., Burns, S.J., Piperno, D.R., Asmerom, Y., Polyak, V.J., Moy, C.M., and Christenson, K., 2004, A 1500-year El Niño/Southern Oscillation and rainfall history for the Isthmus of Panama from speleothem calcite, v. 109, p. D20117.

Lamb, H.H., 1965, The early medieval warm epoch and its sequel.: Palaeogeography, Palaeoclimatology, Palaeoecology, v. 1, p. 13-37.

Leathers, D.J., Yarnal, B., and Palecki, M.A., 1991, The Pacific/North American Teleconnection Pattern and United States Climate. Part I: Regional Temperature and Precipitation Associations: Journal of Climate, v. 4, no. 5, p. 517-528.

Liu, Z., Kennedy, C.D., and Bowen, G.J., 2011, Pacific/North America teleconnection controls on precipitation isotope ratios across the contiguous United States: Earth and Planetary Science Letters, v. 310, p. 319-326.

MacDonald, G.M., and Case, R.A., 2005, Variations in the Pacific Decadal Oscillation over the past millennium: Geophysical Research Letters, v. 32, no. 8, p. L08703.

Mann, M.E., Bradley, R.S., and Hughes, M.K., 1999, Northern hemisphere temperatures during the past millennium: inferences, uncertainties, and limitations.: Geophysical Research Letters, v. 26, p. 759-762.

Mann, M.E., Bradley, R.S., and Hughes, M.K., 1998, Global-scale temperature patterns and climate forcing over the past six centuries: Nature, v. 392, no. 6678, p. 779-787.

Mantua, N.J., Hare, S.R., Zhang, Y., Wallace, J.M., and Francis, R.C., 1997, A Pacific Interdecadal Climate Oscillation with Impacts on Salmon Production: Bulletin of the American Meteorological Society, v. 78, no. 6, p. 1069-1079.

Mantua, N., and Hare, S., 2002, The Pacific Decadal Oscillation, Springer Netherlands 58, 35 p.

Mensing, S., Livingston, S., Barker, P., 2006, Long-term fire history in Great Basin sagebrush reconstructed from macroscopic charcoal in spring sediments, Newark Valley, Nevada. Western North American Naturalist 66, 64–77.

Mensing, S., Smith, J., Burkle Norman, K., and Allan, M., 2008, Extended drought in the Great Basin of western North America in the last two millennia reconstructed from pollen records: Quaternary International, v. 188, no. 1, p. 79-89.

Moy, C.M., Seltzer, G.O., Rodbell, D.T., and Anderson, D.M., 2002, Variability of El Nino/Southern Oscillation activity at millennial timescales during the Holocene epoch: Nature, v. 420, no. 6912, p. 162-165.

National Oceanic and Atmospheric Administration (NOAA), 2010, Palmer Drought Severity Index: http://www.ncdc.noaa.gov/paleo/drought/drght_pdsi.html (September 29 2012).

National Oceanic and Atmospheric Administration (NOAA), 2005, El Niño and La Niña - Related Winter Features Over North America: http://www.cpc.ncep.noaa.gov/products/analysis_monitoring/ensocycle/nawinter.shtml (April 18 2011).

Newman, M., Compo, G.P., and Alexander, M.A., 2003, ENSO-Forced Variability of the Pacific Decadal Oscillation: Journal of Climate, v. 16, no. 23, p. 3853-3857.

Polyak, V.J., and Asmerom, Y., 2001, Late Holocene Climate and Cultural Changes in the Southwestern United States: Science, v. 294, no. 5540, p. 148-151.

Porcelli, D., and Swarzenski, P.W., 2003, The Behavior of U- and Th-series Nuclides in Groundwater: Reviews in Mineralogy and Geochemistry, v. 52, no. 1, p. 317-361.

Prudic, D.E., and Glancy, P.A., 2009, Geochemical investigation of source water to Cave Springs, Great Basin National Park, White Pine County, Nevada: U.S. Geological Survey Scientific Investigations Report 2009–5073, p. 28.

Reinemann, S.A., Porinchu, D.F., Bloom, A.M., Mark, B.G., and Box, J.E., 2009, A multi-proxy paleolimnological reconstruction of Holocene climate conditions in the Great Basin, United States: Quaternary Research, v. 72, no. 3, p. 347-358.

Richards, D.A., and Dorale, J.A., 2003, Uranium-series Chronology and Environmental Applications of Speleothems: Reviews in Mineralogy and Geochemistry, v. 52, no. 1, p. 407-460.

Ropelewski, C.F., and Halpert, M.S., 1986, North American precipitation and temperature patterns associated with the El Niño--Southern Oscillation (ENSO): Monthly Weather Review, v. 114, p. 2352-2362.

Schulz, M., and Mudelsee, M., 2002, REDFIT: estimating red-noise spectra directly from unevenly spaced paleoclimatic time series: Computers & Geosciences, v. 28, no. 3, p. 421-426.

Seager, R., Ting, M., Held, I., et al., 2007, Model Projections of an Imminent Transition to a More Arid Climate in Southwestern North America: Science, v. 316, no. 5828, p. 1181-1184.

Sharp, Z., 2007, Principles of Stable Isotope Geochemistry: Upper Saddle River, NJ, Pearson Prentice Hall.

Smith, J.M., 2003, A 6,500 year pollen record from a wet meadow site in central Nevada. M.S. Thesis, Geography, University of Nevada, Reno.

Stine, S., 1994, Extreme and persistent drought in California and Patagonia during mediaeval time: Nature, v. 369, no. 6481, p. 546-549.

Stine, S., 1990, Late holocene fluctuations of Mono Lake, eastern California: Palaeogeography, Palaeoclimatology, Palaeoecology, v. 78, no. 3-4, p. 333-381.

Torrence, C., and Compo, G.P., 1998, A Practical Guide to Wavelet Analysis: Bulletin of the American Meteorological Society, v. 79, no. 1, p. 61.

Trouet, V., and Taylor, A., 2010, Multi-century variability in the Pacific North American circulation pattern reconstructed from tree rings, Springer Berlin / Heidelberg 35, 953 p.

Van Der Pluijm, Ben A., and Marshak, S., 2004, Earth Structure: 500 Fith Avenue, New York, N.Y., W.W. Norton & Company, Inc.

Wang, C., and Fiedler, P.C., 2006, ENSO variability and the eastern tropical Pacific: A review: Progress in Oceanography, v. 69, no. 2-4, p. 239-266.

Wigand, P., 1997, A late Holocene pollen record from Lower Pahranagat Lake, Southern Nevada, USA: high resolution paleoclimatic records and analysis of environmental responses to climate change.: Proceedings of the Thirteenth Annual Pacific Climate (PACLIM) Workshop, Asilomar, CA, April 14th-17th, 1996. California Department of Water Resources Technical

Report 53 of the Interagency Ecological Program for the Sacramento-San Joaquin Esturary, p. 63-77.

Winograd, I.J., Riggs, A.C., and Coplen, T.B., 1998, The relative contributions of summer and cool-season precipitation to groundwater recharge, Spring Mountains, Nevada, USA, Springer Berlin / Heidelberg 6, 77 p.

VITA

Graduate College
University of Nevada, Las Vegas

Paul Edward Pribyl

Home Address:
5248 Prism Place
Las Vegas, NV 89118

Degrees:
Bachelor of Science, Geology, 2010
University of Wyoming

Thesis Title:
A 2000 year moisture source record from a central Nevada speleothem

Thesis Examination Committee:
Chairperson, Dr. Matthew Lachniet, Ph. D.
Committee Member, Dr. David Kreamer, Ph. D.
Committee Member, Dr. Zhongbo Yu, Ph. D.
Graduate Faculty Representative, Dr. Stan Smith, Ph. D.